CFD ANALYSIS OF A T-38 WING FENCE

THESIS

Daniel Allan Solfelt, Ensign, USN

AFIT/GAE/ENY/07-J19

DEPARTMENT OF THE AIR FORCE
AIR UNIVERSITY

AIR FORCE INSTITUTE OF TECHNOLOGY

Wright-Patterson Air Force Base, Ohio

AFIT/GAE/ENY/07-J19

CFD Analysis of a T-38 Wing Fence

THESIS

Presented to the Faculty

Department of Aeronautics and Astronautics

Graduate School of Engineering and Management

Air Force Institute of Technology

Air University

Air Education and Training Command

In Partial Fulfillment of the Requirements for the

Degree of Master of Science in Aeronautical Engineering

Daniel Allan Solfelt, B.S.A.E.

Ensign, USN

June 2007

AFIT/GAE/ENY/07-J19

CFD Analysis of a T-38 Wing Fence

Daniel Allan Solfelt, B.S.A.E.

Ensign, USN

Approved:

/signed/	5 Jun 2007
LtCol. Raymond C. Maple, PhD (Chairman)	date
/signed/	5 Jun 2007
Dr. Mark F. Reeder (Member)	date
/signed/	5 Jun 2007
Maj Richard D. Branam, PhD (Member)	date

AFIT/GAE/ENY/07-J19

Abstract

A computational study of the effects of a wing fence on the T-38 Talon was performed. RANS simulations were conducted using the CFD solver AVUS to examine the flow around the T-38 and the fence at a Reynolds number of $10x10^6$. The T-38 was modeled as a half aircraft with a symmetry plane down the center line and did not include the empennage. The engine inlet and exhaust were modeled as sink and source boundary conditions using mass flow and pressure specifications. Two fence geometries placed 26" from the wing tip were tested. The first fence, called a simple fence, ran chordwise on the upper surface of the wing. It did not produce significant benefits. The second fence geometry, called the extended fence, wrapped around the leading edge of the wing and produced a 4.9% increase in C_L at 15° angle of attack. It was found that the vortices generated by the fence energized the flow outboard the fence, increasing lift. The extended fence generated vortices significantly stronger than the simple fence, resulting in a higher C_L at 15° angle of attack. These findings indicate that the T-38 high angle of attack performance would be improved by the addition of an extended wing fence.

Acknowledgements

I owe a large debt of gratitude to everybody who supported me through this process. Firstly, to Dr. Hugh Thornburg, who went 'above and beyond' to help me complete this project and also to my advisor, LtCol. Maple, who taught me the basics of CFD. A special thank you goes to Rudy Johnson of AFRL/VAAI who supplied the T-38 CAD data. Also, to my family, my roommate, and my girlfriend, for encouraging me through all of the hard work. Finally, I want to thank God, for the great opportunity to conduct this research.

Daniel Allan Solfelt

Table of Contents

List of Figures

List of Tables

List of Symbols

List of Abbreviations

CFD Analysis of a T-38 Wing Fence

I. Introduction

1.1 T-38 Talon

The T-38 Talon is the primary Air Force jet trainer. It is a twin engine, supersonic fighter, that is known for its ease of maintenance and safety record. The Talon is built by Northrop Grumman and is powered by two J-85-GE-C turbojet engines capable of producing 2900 lbs of thrust and propelling the T-38 to a maximum speed of Mach 1.08. The aircraft has a wingspan of 25' 3" and a length of 46' 4". The first flight was in 1958 and between 1961 and 1972 approximately 1,100 aircraft were delivered of which around 509 remain in service. [18]

Although the T-38 is a proven aircraft, there are several lines of research currently being conducted to improve the Talon's safety, reliability, and flying qualities. The program Pacer Classic is designed to replace aging and outdated engine, avionic, and structural components that could threaten the fleet's reliability and technological relevance to modern jet fighter training. In 2001 Northrop Grumman was given a contract for the Wing Life Improvement Program to design a new wing incorporating fatigue resistant aluminum alloys. Although it has already been in service for over 45 years, the T-38 Talon is expected to remain in service until 2020, due mainly to the aforementioned efforts. [19]

1.1.1 T-38 Stall Characteristics. The T-38 Talon has proven itself over the past 40 years as an effective jet trainer. However, as with almost every system, improvements can and should be made. Examining the flight characteristics of the T-38 sheds light on areas where its performance could be improved. There is current interest for improving the Talon's high AOA performance by increasing the C_L. The T-38 lift curve slope is shown in Figure 1.1

1
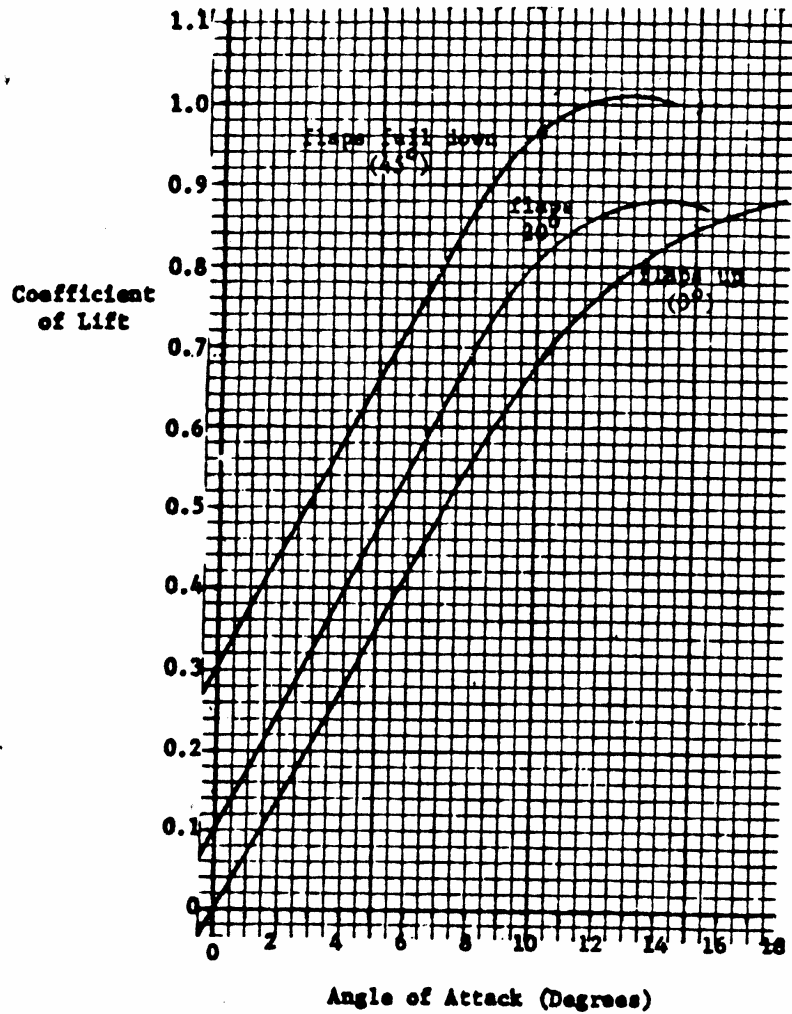
Figure 1.1:   T-38 Lift curve slope for all aircraft configurations [18]

The T-38 $C_{l_{max}}$ with flaps full down is 1.02. The 20° flaps $C_{l_{max}}$ is 0.88. As can be seen in Figure 1.1, the $C_{l_{max}}$ with flaps up is difficult to define. The lift curve slope begins to gradually fall off at around 10° AOA, and there is no clear stall as the AOA increases to 18°. The T-38 flight manual [18] describes the Talon's stall as follows:

! The stall is characterized by airframe buffet and a high sink rate rather than by a clean nose-down pitching motion. As angle of attack is increased, there is corresponding increase in buffet intensity. The buffet is most severe with flaps fully extended. The stall condition is immediately preceded by heavy low-speed buffet and moderate wing rock. The wing rock can be controlled with rudder. The actual stall is normally not accompanied by any abrupt aircraft motion, but is indicated only by the very high sink rate.

1.2   Flow Control

The question arises then, how to improve high AOA flight, without redesigning the entire aircraft or making major adjustments to the existing airframe. The answer lies in flow control. Flow control devices like vortex generators, winglets, and wing fences have been used to improve the aerodynamic performance of hundreds of aircraft. Flow control is commonly added after the final phase of design and production because it can significantly improve the flight characteristics without redesigning the entire vehicle. As early as the 1930's, aircraft employed vane vortex generators, VG, to delay separation. [6, 14] The Beech Starship is a perfect example of this technology. The Beech Starship uses vane vortex generators along the entire span on the wings and vertical stabilizers. The wing VG allows the aircraft to meet its stall requirements, while the VG on the vertical tail provide increased lateral control stability. The VG improved the flight characteristics without significantly changing the airframe [6]

As the T-38 is undergoing Operation Pacer Classic and the Wing Life Improvement program, it is a logical time to investigate the advantages of adding such flow control devices to the T-38. The idea to use a wing fence to improve the performance of the T-38 was originally proposed by the Air Force Test Pilot School. The driving force for considering a wing fence as opposed to vane vortex generators or winglets

was a row of screws that spans the chord of the airfoil 26" from the wingtip. The row of screws exists because of a previous modification to the airframe where a wing section was added to give the T-38 a larger lifting surface. This row of screws provides a relatively easy location to attach a fence without making major structural changes to the wing.

1.2.1 Previous Fence Success. The wing fence has been used on hundreds of aircraft, especially by the Soviets during the Cold War. It was so common that U.S. engineers joked the purpose of the fence on Soviet Aircraft was, "To prevent air from defecting over the tips of the wings." [22] Two cases in which the fence was particularly effective are seen in the SB 13 ARCUS and Vision 87. Both of these aircraft are swept wing like the T-38. [16] The SB 13 experienced favorable spin characteristics with forward positions of the center of gravity. However, if the static margin was less than 10%, the SB 13 experienced a strong wing over roll moment which led to a spin. To investigate this phenomenon, engineers used wing tufts to examine the flow over the wing. A significant cross flow preceding wing stall was observed. To stop the cross flow, two wing fences were tested. The first only ran along the upper surface of the wing and spanned 40% of the chord. It was 150 mm high. This fence did not show significant improvements. The second wing fence was extended around the front of the airfoil. The second wing fence showed considerable improvements and the aircraft could be held in 45° turns without yawing or stalling. The sudden stall and spin were eliminated. [16]

The Vision 87 also had undesirable stall characteristics; so much so that pilots were very reluctant to fly it at high AOA. In light of the success of the SB 13, fences were placed at the half span and flight tests were conducted. The improvements over the initial flight characteristics were large. Not only was the dangerous stall behavior improved, but for practical purposes it was eliminated. In this particular case an unflyable aircraft was transformed into a normal controllable vehicle by attaching

wing fences. "There is probably no better example of the sometimes nearly incredible effectiveness of potential fences." [16]

1.3   Goals of Current Research

Researching the wing fence on the T-38 will be a three tiered approach, utilizing computational fluid dynamics, or CFD, wind tunnel experiments, and actual flight testing. The goal of the current research is to model the wing fence using CFD. The results of the CFD will be compared to the wind tunnel results. Using the information gained during these studies, the safety implications for the T-38, an optimum design for the wing fence will be implemented for actual flight testing.

The goal of this effort is a general improvement of the low speed high AOA flight characteristics of the T-38. Some specific measurements of success might be alleviating the intensity of the wing buffeting during approach, increasing the C_{lmax}, decreasing minimum take off distances, and decreasing stall speed. These effects could be of great advantage to the T-38 because of the nature of its mission. Increasing the safety margin for new pilots being trained on the Talon could save aircraft and lives. Also, there is very little published computational research into the effects of a wing fence on a military jet. Gaining a better understanding of the physics behind the fence will be beneficial not only to the T-38, but also to future aircraft seeking to improve their performance.

II. Background

The primary goal of this research is to improve the low speed, high AOA lift characteristics of the T-38. Flow in this regime is unsteady, turbulent, and beginning to separate. Using CFD to model flow of this nature over a complicated geometry such as the T-38, can be an arduous task. Great care must be taken to set up the problem appropriately to produce accurate results. In order to accomplish this, research into aerodynamic principles, flow control theory, and CFD modeling was conducted and is presented in this chapter.

2.1 Boundary Layer and Stall

The viscous boundary layer is the layer of fluid adjacent to a body, where the momentum and energy is decreased due to viscosity of the fluid. Viscosity is modeled by the no-slip condition, which states flow over a surface has a relative velocity of zero at the surface. The further the flow is from the surface, the less the effects of viscosity are felt, and eventually the velocity in the boundary layer approaches that of the free stream. At the point where the velocity in the boundary layer is 99% of the free stream, designated δ_{99}, the flow can be accurately modeled as inviscid. [4, 15]

There are two basic types of boundary layers, laminar and turbulent. A laminar boundary layer is the region where viscosity has a damping effect on the fluid and the streamlines maintain order. [15] The turbulent boundary layer occurs when the momentum of the flow overcomes the viscosity and causes small, random disturbances. These disturbances grow, interact with one another, and manifest themselves as three dimensional intertwining eddies. [15] The laminar boundary layer has a lower velocity gradient, $\frac{\partial u}{\partial y}$, at the wall when compared to the turbulent boundary layer profile. Since shear stress is proportional to $\frac{\partial u}{\partial y}$ at the wall, the turbulent boundary layer results in a higher skin friction drag. In Figure 2.1 the boundary layer velocity profile on the left is laminar. It has a lower slope when compared to the turbulent boundary layer to its right. [3]
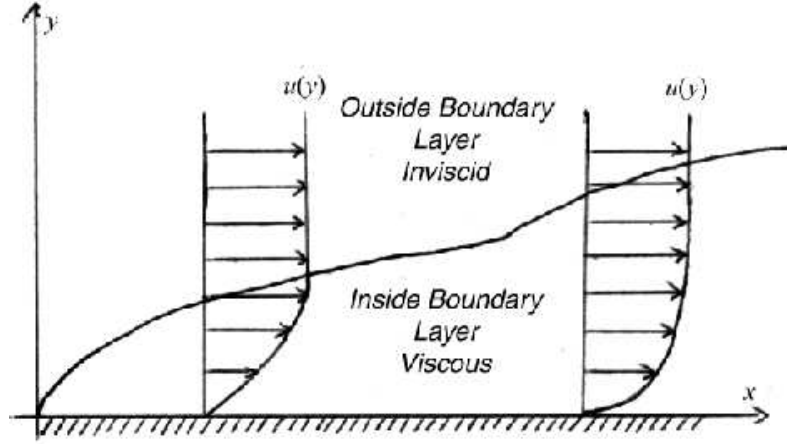
Figure 2.1:   Laminar and turbulent boundary layer [5]

Flow inside the boundary layer is especially sensitive to the adverse pressure gradient. An adverse pressure gradient is defined as $\frac{\partial p}{\partial x} > 0$, when x increases in the downstream direction. A positive pressure gradient retards or decelerates the flow. Flow inside the boundary layer is affected more than flow outside the boundary layer because its energy has already been degraded from losses due to friction. Outside of the boundary layer the fluid still experiences an adverse pressure gradient, but generally has enough energy to overcome the restricting forces. Figure 2.2 demonstrates the effects of the adverse pressure gradient. [15]

The deceleration of the flow results in a loss of forward momentum. Flow continues to lose energy as it moves through the adverse pressure gradient until it reaches a point where the slope of the velocity profile at the surface is zero and separation occurs.

$$\left(\frac{\partial u}{\partial y} \right)_{y=0} = 0 \tag{2.1}$$

Equation 2.1 is the mathematical definition of the separation point. The separation point can be seen in Figure 2.2 at point P_2. Flow separation drastically alters the pressure distribution around an airfoil. When flow separation occurs over a large portion of an airfoil, it stalls. A stall results in a large decrease in lift, increase in

7
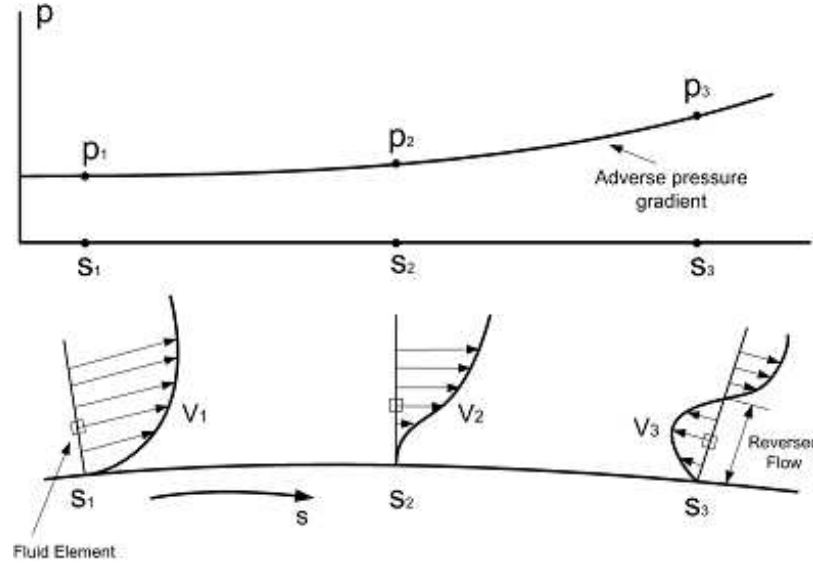
Figure 2.2:   Adverse Pressure Gradient [5]

pressure drag, and change in pitching moment. Stall on an airfoil is shown in Figure 2.3. [3]

The boundary layer type on an aerodynamic surface influences stall. Since flow separation begins with the boundary layer, the higher the velocity gradient near the surface, the more energy it will have to resist separation. A turbulent boundary layer will remain attached to a surface longer than a laminar boundary layer because it has a higher velocity gradient near the surface. [3, 4]

2.2   Flow Control

Many flow control devices are based on the principle of energizing the boundary layer. There are two types of flow control, active and passive. The difference between these two methods is evident in their respective names. Passive flow control uses inert objects that manipulate flow by their physical shape. Some common passive flow control devices are vortex generators, fences, high lift flaps, and winglets. Active flow control injects the boundary layer with energy from small jets of air powered by internal structure. [21] Both active and passive flow control methods have shown effectiveness in delaying separation, increasing control power, or reducing drag. However,

CHORD LINE

ANGLE OF ATTACK

RELATIVE WIND

ANGLE OF ATTACK

CHORD LINE

STALL

ANGLE OF ATTACK

RELATIVE WIND
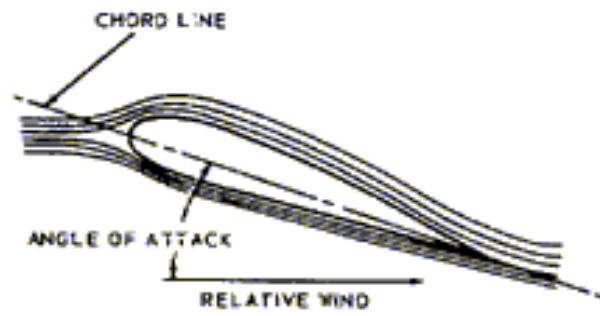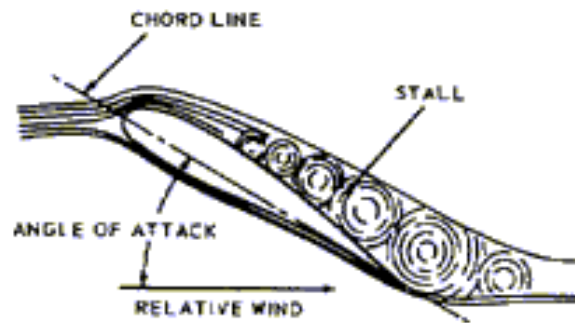
AIRFOIL ANGLES OF ATTACK VS LIFT

SCHEMATIC DIAGRAM ILLUSTRATING STALL

Figure 2.3:   Stall visualization [20]

9

since active flow control devices are complex, difficult to maintain, and expensive, only passive flow control was considered for the T-38. [14]

The wing fence was chosen for the current effort for two reasons. The first reason is because of the past success of the wing fence in improving high AOA performance. Some examples were discussed in Chapter I. Second, the T-38 contains a row of screws on the upper surface of the wing 26" from the wing tip, which presents an ideal location to test the effectiveness of the wing fence without significantly altering the airframe. Even simple vane vortex generators would require punctures or welds to the wing surface. The fence, however, can be attached and removed with no permanent alterations to the structure.

2.3 Wing Fence

The wing fence produces a complicated interaction of several factors working together to increase lift at high AOA. Research proved to be a challenge, because there was no source stating one all inclusive theory on why a fence works. One source concentrated on the fence's vortex generating capabilities. [23] Another explained the fence's effects come through its ability to alter the potential flow around the wing in a way that lift is increased at high AOA. [16] This section provides an overview of several theories to gain insight into what is actually happening around the fence.

A wing fence is commonly referred to as a boundary layer fence, potential fence, or just fence. A wing fence is essentially a thin plate, with height roughly proportional to the local wing thickness, running chordwise in the direction of flow. Figure 2.4 shows a typical fence on a Russian MIG.

The wing fence, or boundary layer fence as it was referred to during its creation, was invented in 1938 by Wolfgang Liebe. [16] The motivation for the wing fence came from the Messerschmitt Bf 109. The Bf 109 was a straight wing aircraft which experienced severe wingtip stall. German engineers initially used retractable Handley Page slats to alleviate the stall, but these devices were very expensive. To investigate

Figure 2.4:   Russian Mig-21 with fence. [22]

alternative methods of fixing the Bf 109's stall characteristics, wing tufts were glued onto the upper surface of the wing and photographs were taken during flight to examine the flow. An interesting stall pattern was observed. The stall originated near the fuselage and was followed by a cross flow of 'wake material' that rushed towards the low pressure on the leading edge. It took one second for this flow to reach the wingtip and produce a separation over the whole wing. [16] Wolfgang Liebe stated, "One gets the impression that the stall is not enforced by the local angle of attack, but that it is caused by the penetration of the cross flow. So a barrier set in the penetration path should be able to stop this from happening. From this idea the boundary layer fence was born." [16] The wing fence was installed on the Bf 109 and immediately the stall characteristics improved.

Liebe's initial study led him to believe the wing fence worked solely because it stopped cross flow in the boundary layer. However, this idea was flawed. The boundary layer is typically only a few millimeters thick, and even in the separated region on the wing, it is only a few centimeters. The cross flow inside the boundary layer is of the same magnitude. If slowing the cross flow contained in the boundary layer was the only mechanism by which a fence worked, the fence should only need to be about the size of the boundary layer. However, research has proven in order to be effective, a fence must be many times larger than the boundary layer. Another reason why Liebe was not fully correct is the boundary layer grows as it travels along a surface. If the sole purpose of the fence was to stop crossflow, the the fence should

11
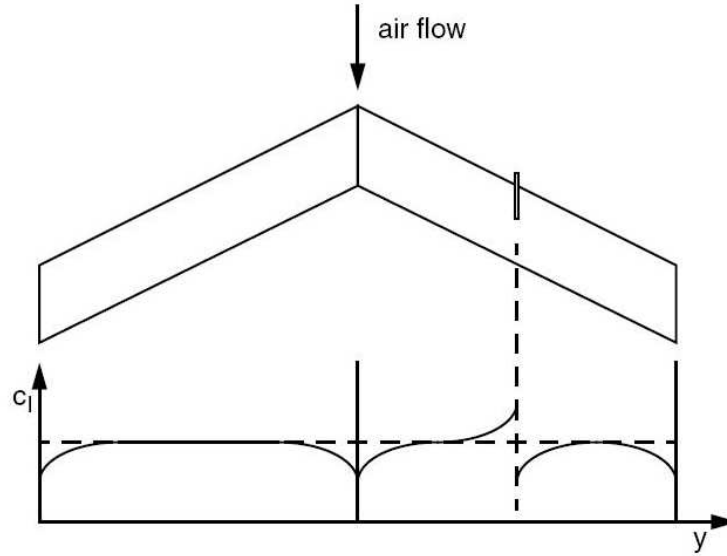
Figure 2.5: C_l distribution on a wing with an idealized fence [16]

be most important in the back of the wing where the boundary layer is the thickest. Testing has shown extending a fence in this region does not produce significant benefits. Thus, delaying cross flow in the boundary layer is not the only mechanism of the fence. [16]

2.3.1 *Wing Fence and Potential Flow.* Dr. Karl Nickels' book, "Tailless Aircraft," contains a large section about wing fences on swept wing aircraft. [16] He explains the fence can be best understood if it is considered to be a thin infinite wall placed along the span of a finite wing. The idealized fence changes the lift load distribution. This effect is shown in Figure 2.5.

According to Dr. Nickels, the effect of the wing fence is to increase the C_l load inboard of the wing fence, and to decrease it outboard of the fence. This delays wingtip stall. Thus, the primary operating mechanism of a wing fence is not merely stopping the cross flow of the boundary layer, but changing the lift distribution. Since lift distribution around a wing can be determined by the potential flow, the wing fence is commonly referred to as a potential fence. [16]

A few points need to be highlighted to avoid any misunderstandings regarding this conceptual approach to the wing fence. The first is separation at high AOA is an effect of the boundary layer, and slowing the cross flow does have an effect. The wing fence influences the boundary layer, and consequently stall, but, the effectiveness of a fence is not directly in its control of the boundary layer. Nickel states his theory as follows: "Their effectiveness comes indirectly from influencing the potential flow. Namely, the flow conditions at the wings are changed in such a way that the Cl load of the wingtips is reduced. Thus the boundary layer in the region remains "sound" much longer, which avoids a separation and a local stall." [16]

2.3.2 Wing Fence as a Vortex Generator. Examining the wing fence as an infinite wall is effective for understanding its overall effects. However, a real wing fence is not an infinite wall and thus it must affect the flow through some physical mechanism. This real effect is vortex generation.

A VG is a flow control device used to delay separation. The most common type is the vane VG. [8] It is typically in the shape of a small airfoil or thin plane that protrudes from a surface, and is positioned at an incidence angle to the oncoming flow, which causes vortex generation. The vortex captures energy from the free stream and transfers it to the boundary layer, delaying separation. [14] The vortex can persist for hundreds of times the length of the boundary layer, delaying the separation point on the airfoil significantly. There are many types of VG, varying in shape, size and location, but they all operate on the same principles as the vane VG.

Dr. Zhidkosti conducted wind tunnel research into fence vortices in his publication, "Flow On A Swept Wing in the Region of a Fence." [23] On a wing swept at 55°, he found the wing fence produces two vortices. The first vortex was formed on the upper portion of the fence on the inboard side. The fence vortex is caused by a pressure differential across the fence. The strength of the fence vortex is influenced heavily by AOA and the yaw angle, and is strongest when these angles are large. The vortex changed the pressure distribution over the wing, causing a new pressure

minimum inboard of the fence. Zhidkosti did not comment on the location or source of the second vortex, but did state it alters the flow pattern near the wing and causes significant restructuring of the velocity field that could affect the performance of the horizontal tail. [23] The final result of his research was the fence caused flow to remain attached outboard of the fence even after separation occurred inboard of it.

2.4   Computational Theory

A wing fence is most effective at high AOA, when flow is turbulent, unsteady, and beginning to separate. [23] Using CFD to model this is not a simple process. An understanding of the mathematical principles and techniques involved is necessary to produce valuable results.

The governing equations for a Newtonian fluid are called the Navier Stokes, or N-S equations. They are a set of five coupled, non linear, partial differential equations. There is no closed form solution. Mathematical manipulation and assumptions are made to simplify the N-S equations. [15]

2.4.1   Turbulence.   Turbulent flow is unsteady, viscous, and complex combination of three dimensional interacting eddies. [15] It is not a fluid property but rather a property of the flow. The energy contained in a turbulent flow is distributed through eddy size. The large scale eddies carry most of the kinetic energy where as the smallest scale eddies convert their kinetic energy to heat through viscous or molecular dissipation. [15] The Navier Stokes equations can be used to directly model turbulent flows. This type of computation is called Direct Numerical Simulation or DNS. In order to do this, however, the grid spacing must be less than the smallest scale turbulent eddies. For complex high Reynolds numbers flows this requires enormous memory and computational power that current technology does not support. Therefore, simplifications must be made to the Navier Stokes equations.

The most common technique is called Reynolds Averaged Navier Stokes or RANS. Reynolds averaging uses the definition of the average integral to resolve the

flow variables in the N-S equations into time averaged and turbulent fluctuation terms. A simplified explanation of Reynolds averaging is as follows. The velocity of turbulent flow can be written as an average velocity plus a fluctuation term.

$$u_i = \bar{u}_i + u_i' \tag{2.2}$$

Applying the definition of velocity and averaging the Navier Stokes equations using spatial or temporal techniques yields a new set of equations and six new correlation factors called the Reynolds stresses. The Reynolds averaged equations for momentum and mass are included in Equations 2.3 and 2.4. The average fluctuation terms are assumed to be zero. [7,15] The energy equation is derived in similar manner.

$$Mass: \frac{\partial \bar{\rho}}{\partial t} + \frac{\partial}{\partial x_i}\left(\bar{\rho}u_i + \rho u_i'\right) = 0 \tag{2.3}$$

$$Momentum: \frac{\partial \bar{\rho}\bar{u}_i}{\partial t} + \frac{\partial}{\partial x_j}\left(\overline{\rho u_i}\bar{u}_j\right) = -\frac{\partial \bar{P}}{\partial x_i} + \frac{\partial}{\partial x_j}\left(\bar{\tau}_{ij} - \bar{\rho}\overline{u_i'u_j'}\right) \tag{2.4}$$

where

$$\bar{\tau}_{ij} = 2\mu \bar{S}_{ij} - \frac{2}{3}\mu \frac{\partial \bar{u}_k}{\partial x_k}\delta_{ij} \tag{2.5}$$

$$\bar{S}_{ij} = \frac{1}{2}\left(\frac{\partial \bar{u}_i}{\partial x_j} + \frac{\partial \bar{u}_j}{\partial x_i}\right)$$

The Reynolds stresses are six new unknowns. These initially seem to make the computations more complicated. However, the velocity and flow parameters can now be described in terms of average quantities. Turbulence models are used to close the RANS equations. [15] The most common method for closing the RANS equations was proposed by Boussinesq in 1877. Boussinesq theorized the Reynolds stresses are proportional to the local mean flow strain rate, and thus are similar in form to viscous stresses. [15] The resulting equation is shown in Equation 2.6.

15

$$\bar{\tau}_{ij}^T = -\overline{\rho u_i u_j} = 2\mu_T \bar{S}_{ij} - \frac{2}{3}\mu_T \frac{\partial \bar{u}_k}{\partial x_k}\delta_{ij} \qquad (2.6)$$

The μ_T term is the turbulent eddy viscosity. Instead of solving for the six Reynolds stresses, now only the μ_T term must be computed. Since the eddy viscosity is a property of the flow and not of the fluid it must be computed at every point in the flow. Turbulence models based on the Boussinesq approximation are semi-empirical algebraic or differential equation formulations that solve for the turbulent eddy viscosity. [15, 21] Different turbulence models are applicable to different types of flow. Algebraic models are typically used for flow with small variations in turbulent length scale, such as attached boundary layers. For separated flows characterized by a wide range of length scales, a one or two differential equation model is appropriate. [15]

The turbulence model used in this research is the Spalart-Allmaras RANS differential equation formulation. The S-A model solves for a variable dependent on turbulent viscosity. The model is based on empiricism, Galilean invariance, dimensional analysis and dependence on molecular viscosity. [7, 15] The model uses a wall destruction term that reduces the turbulent viscosity in the laminar sublayer and trip terms to smoothly transition from laminar to turbulent flow. The S-A model is given in Equation 2.7 beginning with the transport equation for the variable $\tilde{\nu}$. The remaining equations deal with production, diffusion of the Reynolds stresses, turbulent dissipation and the definition of the constants. [15]

$$\frac{\partial \tilde{\nu}}{\partial t} + u_i \frac{\partial \tilde{\nu}}{\partial x_i} = c_{b1}\tilde{S}\tilde{\nu} + \frac{1}{\sigma}\left[\nabla \cdot \left((\nu + \tilde{\nu})\nabla\tilde{\nu}\right) + c_{b2}\left(\nabla\tilde{\nu}\right)^2\right] - c_{w1}f_w\left(\frac{\tilde{\nu}}{d_w}\right)^2 \qquad (2.7)$$

$$\nu_t = f_{v1}\tilde{\nu}$$

$$\tilde{S} = f_{v3}S + \frac{\tilde{\nu}}{\kappa^2 d_w{}^2} f_{v2}$$

$$S = \left| \frac{\partial u_i}{\partial x_j} - \frac{\partial u_j}{\partial x_i} \right|$$

$$\chi = \frac{\tilde{\nu}}{\nu}$$

$$f_{v1} = \frac{\chi^3}{\chi^3 + c_{v1}{}^3}$$

$$f_{v2} = \left(1 + \frac{\chi}{c_{v2}} \right)^{-3}$$

$$f_{v3} = \frac{(1 + \chi f_{v1})(1 - f_{v2})}{max(\chi, 0.001)}$$

$$f_w = \left(\frac{1 + c_{w3}{}^6}{g^6 + c_{w3}{}^6} \right)^{1/6}$$

$$g = r + c_{w2}(r^6 - r)$$

$$r = \frac{\tilde{\nu}}{\tilde{S}\kappa^2 d_w{}^2}$$

$$c_{b1} = 0.1355, \ \sigma = 2/3, \ c_{b2} = 0.622, \ \kappa = 0.41$$

$$c_{v1} = 7.1, \ c_{v2} = 5$$

$$c_{w1} = \frac{c_{b1}}{\kappa^2} + \frac{(1 + c_{b2})}{\sigma} = 7.1$$

$$c_{w2} = 0.3, \ c_{w3} = 2$$

2.5 Previous Research

To determine the best approach for the current study, research was conducted to find current methods for modeling high AOA and passive flow control. The most current data has shown DES, when compared to RANS solutions for separated flow, more accurately captures unsteady effects. [9–12] However, producing a DES grid is

a complicated, time consuming task. Also, the cost of a DES solution is much higher than a RANS solution. Before employing DES, researchers should ensure DES will provide more pertinent data than other more efficient and less expensive models. In the research led by James R. Forsythe, which studied the F-15E at high AOA, [11] RANS and DES solutions were computed for the F-15E and compared closely. Three grids were built from a baseline grid of 5 x 10^6 cells, with the finest grid containing 11 x 10^6 cells. The researchers were surprised to find RANS solutions for the lift, pitching and drag data produced accurate results when compared to the Boeing data base. DES yielded only slightly more accurate predictions. The downside to the RANS solutions was they did not accurately capture significant unsteadiness. However, mean flow data for both the DES and RANS solutions was accurate. The DES solutions were also significantly effected by the grid density, but the RANS lift, moment, and drag data only varied by 1% from the baseline to fine grid. [11, 12]

John A. Ekaterinaris used RANS modeling to investigate vane vortex generators on a wing. [21] Results demonstrated RANS solutions were adequate to determine VG can reduce flow separation. RANS was able to detect jet effects in the boundary layer, pressure distribution alterations, and the changes in VG effectiveness due to incidence angle and placement. [21]

The results of these studies seem to justify using RANS to investigate the wing fence. Although a DES simulation will capture some of the unsteady effects of the fence RANS will not, the main thrust of this effort is to analyze the mean effects of the fence on the lift. These studies demonstrate RANS can accomplish this. Due to time and expense constraints, along with the success of similar studies, this research is justified in using RANS solutions.

III. Methodology

The success of this study relies not only on the quality of the CFD set up, but also on carefully matched simulations of realistic flight conditions for the T-38. Great care was taken to create a relevant test matrix with accurate boundary conditions. The solver used in this study is the Air Vehicles Unstructured Solver, AVUS. AVUS will be discussed in subsequent sections.

3.1 Test Matrix

The test matrix was developed by examining the T-38 flight profile. Since the goal is to investigate the effects of the fence at low speed and high angle of attack, tests are concentrated in this regime. The most common time the T-38 experiences these conditions occurs during landing. As the T-38 turns into final approach, it slows to a baseline speed of 155 knots plus 1 knot per 100 pounds of remaining fuel over 1000 pounds. [18] The T-38 will commonly approach anywhere from 155-175 knots. The throttle setting during final approach is 91%. During the flare the throttle is set to idle. Flare and touchdown occur anywhere from 10-20 knots below the final approach speed. [18]

To mimic the typical T-38 landing pattern at sea level, three tests were conducted between $0 - 10°$ AOA, 170 knots, and 91% power. To recreate conditions around the flare, one test was run for $15°$ AOA, 150 knots, with the engine at idle. Ground effect was not modeled. Although ground effect has an influence during the flare, the goal in this research is not merely to recreate landing, but to investigate the generic effects of the fence. Modeling the test cases after the landing profile is a tool to produce realistic scenarios. The test matrix is shown in Table 3.1.

Table 3.1:   Test Matrix

AOA	Throttle Setting	Mach	Altitude (ft)	Flight Condition
0	91%	0.25	Sea Level	Final
5	91%	0.25	Sea Level	Final
10	91%	0.25	Sea Level	Final
15	idle	0.2	Sea Level	Flare/Stall

3.2 T-38 Geometry

The T-38 is modeled as a half aircraft with a symmetry plane cutting down its centerline. Justification for this model came from Dr. Forsthye's study of the F-15 at high AOA that found no significant difference between modeling the full or half aircraft. [11] The T-38 is modeled without empennage since the initial CAD data did not include the tail section. The removal of the empennage will clearly have an effect on the final solution. However, most of the lift contribution comes from the wings and fuselage and not the empennage. Since this research is concerned only with changes in lift due to the fence, matching the C_L of the computational model to the real aircraft C_L is not critical. Another concern with the cut off empennage is it creates an unrealistic pressure drag and flow that could negatively influence the solution. However, any negative effects will be minimal because the cut off occurs approximately 2 root chord lengths from the area of interest near the fence and any detrimental influence will be felt equally for each test.

3.2.1 Fence and Flap Geometry. The wing fence was inserted 26" from the wing tip. Two fence geometries were tested. The first fence, called a simple fence, begins 2" behind the leading edge and continues to the trailing edge, a distance of 43". The simple fence is a constant 2.5" high, as measured from the upper wing surface to the top of the fence. It has a thickness of 0.5" in its center and a constant taper down to a sharp leading and trailing edge. In the actual fabrication on the aircraft the fence will not have a sharp leading and trailing edge. It will be a constant thickness along the chord. However, to avoid an extremely high number of grid points necessary to capture the effects of blunt fence edges, sharp intersections were used. The simple fence is pictured in Figure 3.1

The second fence shares the same width and height dimensions, but was extended around the leading edge. Instead of continuing to the back of the wing like the simple fence, it was cut off 7" before the trailing edge. This study will refer to this fence as the extended fence. The motivation for extended fence design is research has
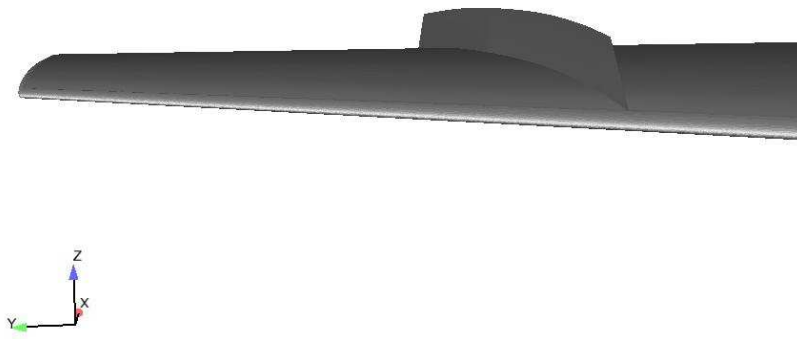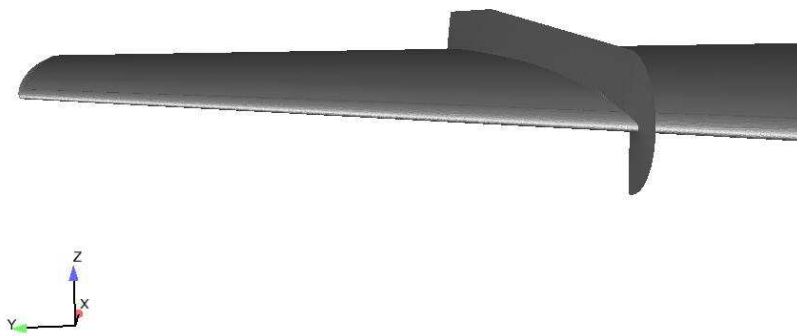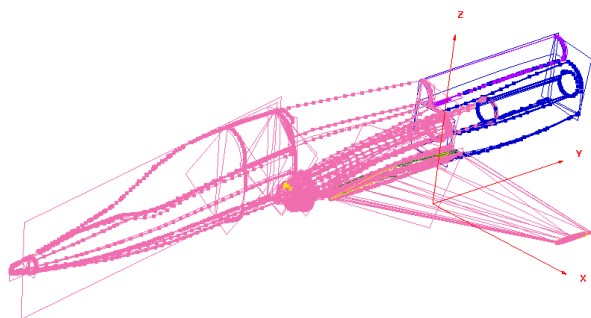
Figure 3.1:   Simple fence.

Figure 3.2:   Extended fence.

demonstrated that if a fence only on the upper surface of a wing is minimally effective, wrapping it around the leading edge can significantly improve its performance. [16] The extended fence is displayed in Figure 3.2.

3.3   RANS Grid Generation

Grids were generated in a two stage process using the programs Gridgen™ and Solidmesh™. The first step was generating the surface mesh on the T-38. This proved to be an arduous and time consuming task. The initial CAD data supplied by the test engineers was a complicated, unlayered combination of trim surfaces, biconvex surfaces, and lines. Simply determining which database elements were actually used in defining the surface was a lengthy process. Even after the useful entities were gleaned from the CAD data, many surfaces did not have a clean intersection. In several areas these errors made determining the exact intersection of two surfaces impossible and the surface in the gap had to be estimated. Fortunately, the gaps were small, on the order of tenths of an inch to half an inch of surface variation. To bridge the gaps one of the two misaligned surfaces was chosen to represent the aircraft surface and a domain was laid from the chosen surface over the gap onto the other data base entity. Most of the intersection problems were on the fuselage and engine cowling, away from the fence, so their impact on the final solution is negligible, however, worth noting. The initial CAD data and the final baseline surface domains for these are shown in Figure 3.3.

3.3.1   *Surface Mesh Attributes.*   Since computational cost and time are important factors, a uniform, high concentration of cells on the surface mesh was not practical. In areas where the aircraft geometry was relatively simple and would not have a large effect on the flow near the fence, fewer cells were placed. Around the engine inlet, leading edge, and fence, a much higher concentration of cells in the surface mesh was tolerated.

(a)
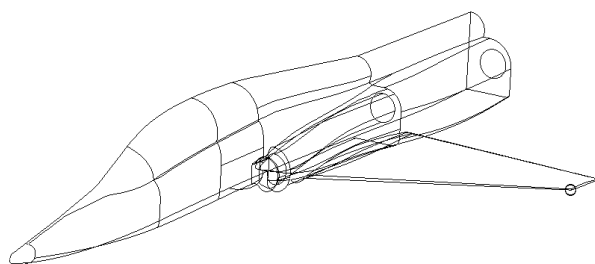
(b)

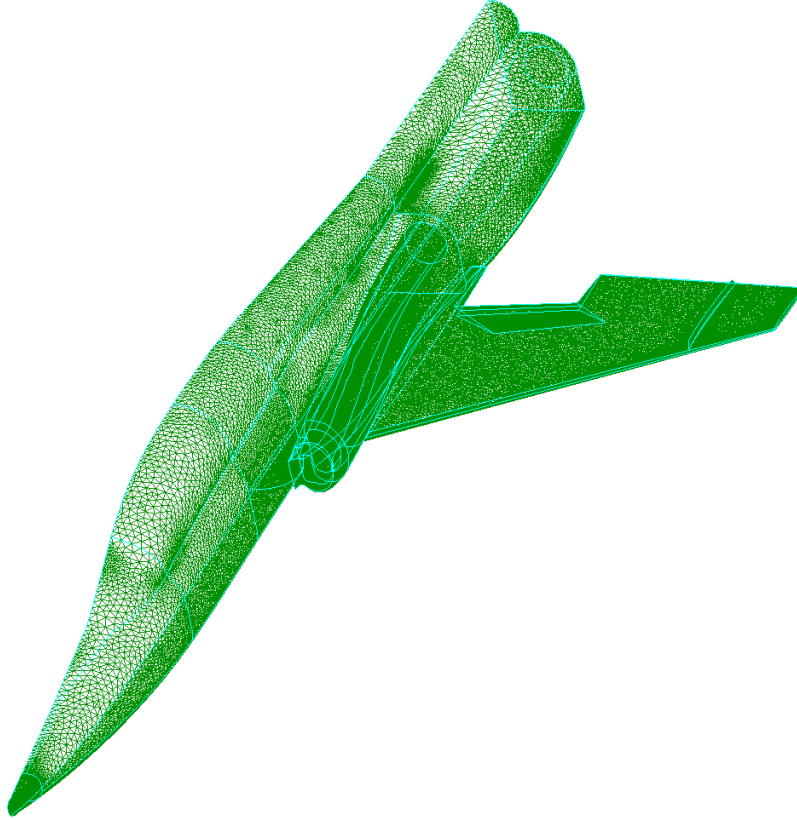Figure 3.3:   (a) Initial CAD data.(b) Final surfaces.

Figure 3.4:   Baseline surface mesh with a simple fence.

Four baseline surface meshes were created. All four grids contained approximately 200,000 cells with similar spacing. The grids used for the fence had a higher concentration of cells around the fence, but maintained the same spacing in other areas. The first mesh had no fence or flaps deployed and is referred to as the clean configuration. Another mesh was generated with flaps deployed at 45°. Finally, one baseline surface mesh for the simple fence grid and one for the extended fence were created. Figure 3.4 shows the simple fence baseline surface mesh. One fine surface mesh was generated for the extended fence case to test the influence of grid density. A cell concentration three times higher than the baseline was used for the fence and the wing while the fuselage cell density remained unchanged. This resulted in final surface grid of 295,000 cells.
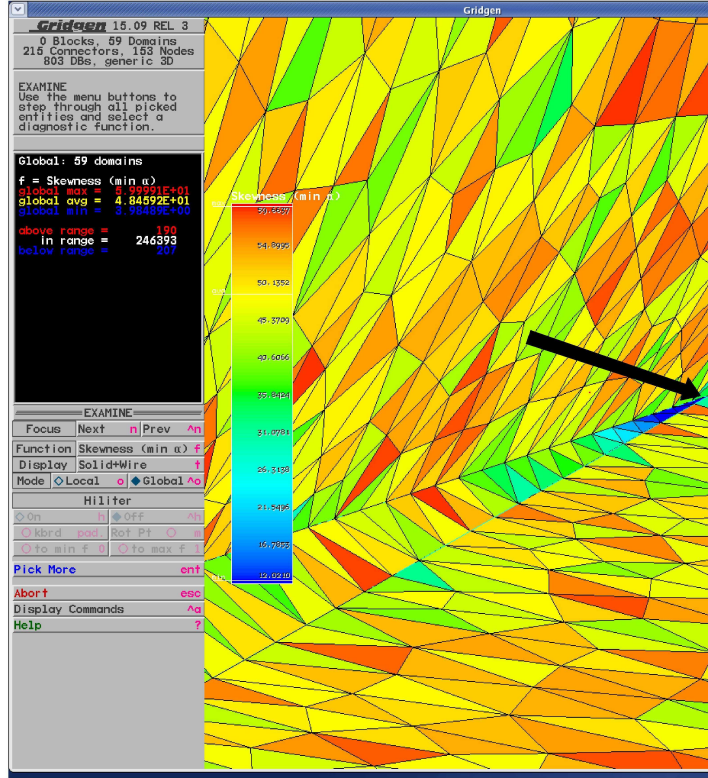
Figure 3.5:   Surface domains intersecting at a small angle.

In order to maintain a high quality surface grid the goal for cell skewness was to avoid cells of less than 20 degrees minimum angle. This condition was violated in several instances. The difficulty was the final surface mesh contained 59 domains which intersected at a wide range of angles. When two domains intersect at an angle less than $20°$, there will always be at least one cell with an angle equal to the intersection angle. An example of a small surface domain cell angle on the fuselage is shown in Figure 3.5.

Each surface mesh had approximately 200 cells with an angle less than $20°$ with a minimum angle of $4°$. This was a relatively small number since each surface mesh contained around 200,000 cells. Almost all of the skewed cells were on the fuselage, in areas of low surface curvature with minimal influence to the area of interest on the wing. As a result, the skewed cells were tolerated.

3.3.2   Volume Grid Generation.   After generating the surface mesh in Gridgen™ the grids were exported as Nastran files and loaded into Solidmesh™ for volume grid generation. Solidmesh™ uses an Advancing-Front/Local-Reconnection 3-D unstructured grid generator. [1] The boundary layer was grown using a $y+ = 1.5$, a reference Reynolds number of 10 x 10^6 calculated from the root chord, and a growth rate of 1.2. The resulting initial spacing was 0.0002". The volume mesh growth rate was also set to 1.2. All baseline volume grids were generated using the same settings. The final cell count in each grid was approximately 5.5 x 10^6. The fine grid was generated using interpolation in the boundary layer and volume mesh resulting in a final grid containing 12.5 x 10^6 cells.

3.3.3   Boundary Conditions.   The boundary conditions were set using the AVUS grid interface program Blacksmith. The Solidmesh™ grids were read into Blacksmith, rotated into the Panair coordinate system, and scaled from inches to meters. The Panair coordinate system has X pointing out the back of the aircraft, Y out the right wing and Z up through the canopy. All cases are modeled as out of ground effect. This is accomplished by utilizing the farfield boundary condition for the five sides of the bounding rectangle away from the T-38 and a slip wall on the symmetry plane. The farfield surfaces were located 5 times the aircraft length in front of the nose, 6 behind the tail, 5 above and below, and 5 out the right wing. The aircraft surfaces were modeled as walls with a no slip adiabatic condition. The engine inlet and exhaust were set as a sink and a source, respectively.

The farfield boundary condition in AVUS was set to the fixed option, which holds all variables at the user specified values where flow enters the domain. When flow leaves the domain, the values are allowed to float. The solid wall no-slip condition utilized an adiabatic assumption and specified a zero velocity on the wall. The solver assumes the normal pressure and density gradients are zero. Since AVUS does not have an explicit symmetry plane boundary condition the symmetry plane was set using a solid wall with a slip condition. The source, or engine exhaust, was a total

Table 3.2:   Inlet and Exhaust Boundary Conditions

Throttle	Inlet(Sink)	Exhaust(Source)	
	Massflow $\frac{kg}{s}$	T-Total(k)	P-Total(Pa)
Idle	6.69	791	104109
91%	17.34	750	154304
Max	9.52	1970	97905

pressure setting that required the total pressure, temperature, and Mach number. The inlet was specified as a sink massflow in $\frac{kg}{s}$

Table 3.2 shows the engine settings that defined the boundary conditions used for the source and sink at the various throttle settings. This data was supplied courtesy of the Air Force Test Pilot School.

3.4   AVUS

Solutions were computed using AVUS, or Air Vehicles Unstructured Solver. AVUS's fundamental coding is finite-volume, cell centered, and first order accurate in time and space. Second order accuracy in space is achieved by assuming flow varies linearly within each cell. Second order in time is computed by using an unconditionally stable point implicit scheme developed by Tomaro et al. [2] The turbulence model implemented in this research is the one differential equation Spalart-Allmaras model. Results and visualizations were produced using Ensight™, Fieldview™, and Matlab™.

IV. Results

The results in this chapter focus on the influence of the fence on the lift. In light of the ambiguity in the research presented in Chapter 2 on how a wing fence works, the analysis in this section will take a broad approach. Instead of attempting to match the results to the accepted theories, the data will speak for itself. It will of course be compared to the theories in Chapter 2, but it will also investigate new ideas and possibilities for the physics behind the wing fence.

It is important to make one point before presenting the results. In the course of the study, the influence of grid density on the solution was found to be minimal. As an example, at $10°$ AOA the change in C_L from the baseline extended fence grid to the high density fence grid was only 0.1%. At $15°$ AOA the solutions varied by only 1%. Since the solutions and visualizations were so close to one another, comparisons between the baseline and fine grids are valid.

4.1 Model Validation

An average y+ value of 1.5 was achieved in the boundary layer. This was determined from the AVUS output files. Convergence was determined by analyzing the force data and residuals. Each test ran 5000 iterations. The residuals in each case were reduced by three orders of magnitude and the forces converged by 4500 iterations. Table 4.1 compares the CFD results to experimental results from the lift curve slope in Figure 1.1. For AOA greater than $0°$, the experimental and CFD results are surprisingly close. Even without the empennage the lift data from the CFD solutions between $5 - 10°$ were only between 1-3% different from the experimental results. This is likely due to the fact that at lower AOA, the empennage plays a smaller role in lift. At $15°$ the flap only CFD results were 10% higher than the experimental data. The importance of these comparisons is it validates the data produced by the CFD is not only converging to a solution, but the solution reflects the real aircraft.

Table 4.1: C_L convergence

AOA	Exp. Clean Config.	CFD Clean Config.	Exp. Flap Only	CFD Flap Only
0°	0	0.15	0.3	0.414
5°	0.34	0.35	0.68	0.717
10°	0.71	0.7	0.95	0.979
15°	-	-	1.0	1.111

4.2 C_L Results

The C_L computed for each test is shown in Table 4.2. The extended fence was not tested at 0° and 5°.

Table 4.2: C_L Results

AOA	Flap Only	Simple Fence	Extended Fence	Ex. Fence Dense Grid
0°	0.414	0.4231	-	-
5°	0.714	0.717	-	-
10°	0.9645	0.979	0.9756	0.9755
15°	1.101	1.111	1.147	1.159

The largest increase in C_L was 4.9% at 15° AOA in the fine extended fence grid. The baseline extended fence increased C_L by 3.9% and the simple fence increased it 0.9%. At 10° the simple fence increased C_L 1.4% and the extended fence increased C_L 1.2% in both the baseline and dense grids. Neither fence caused significant change in C_L below 10° AOA.

In order to determine the cause of the change in C_L, the flow structure around the fence was examined carefully and compared to the theory outlined in Chapter 2.

4.3   X Plane Views

The first step in analyzing the results is to gain an understanding of the large picture of what the fence is doing to the flow. Once this is determined, it will allow the areas of interest to be investigated more thoroughly with different numerical and visualization techniques.

A cut plane was inserted through the wing in the spanwise direction through the center chord and colored with pressure and in-plane velocity vectors. This view will begin to reveal vortices, low pressure regions, and general areas of influence of the fence. Since the greatest effect of the fence is at $10°$ and $15°$, the analysis of the wing fence will concentrate in this region. All comparisons are made to the baseline flap-only grid since all fence grids have flaps deployed.

The X cut planes are shown in Figures 4.1 through 4.4. These figures compare the simple and extended fence to their corresponding flaps-only solution for $10°$ and $15°$ AOA. For ease of viewing, the fence and flaps-only cases at each AOA are included together. Pressure color and vector length scales are the same for all plots.

Figures 4.1 through 4.4 give a useful perspective of the flow. A cursory viewing immediately reveals the fence has a significant effect. The flaps only cases, at every AOA, have a smooth pressure distribution above the wing. The in-plane velocity vectors show a spanwise flow on the upper surface and the expected circulation around the wingtip from high to low pressure. The fence drastically changes this picture. Immediately evident, especially in the cases at $15°$ AOA, is a change in the pressure distribution. Instead of a steady change in the pressure above the wing, pressure is essentially divided into two regions. The first begins at the wingtip and continues half of the distance to the fence. This pressure is lower than the corresponding pressure with no fence at the same location. The second begins at the fence and extends towards the fuselage. The second low pressure region appears to be very close in shape to the case with no fence and slightly lower in pressure.

The in-plane velocity vectors indicate the low pressure regions in the presence of a fence are closely tied to vortices. This is observed in Figure 4.5, which shows two regions of swirling velocity vectors indicating two vortices. The first corresponds to the low pressure region near the wing tip and the second remains close to the outboard side of the fence. This discussion will refer to the vortex towards the wing tip as the tip vortex and the vortex straddling the fence as the fence vortex. The
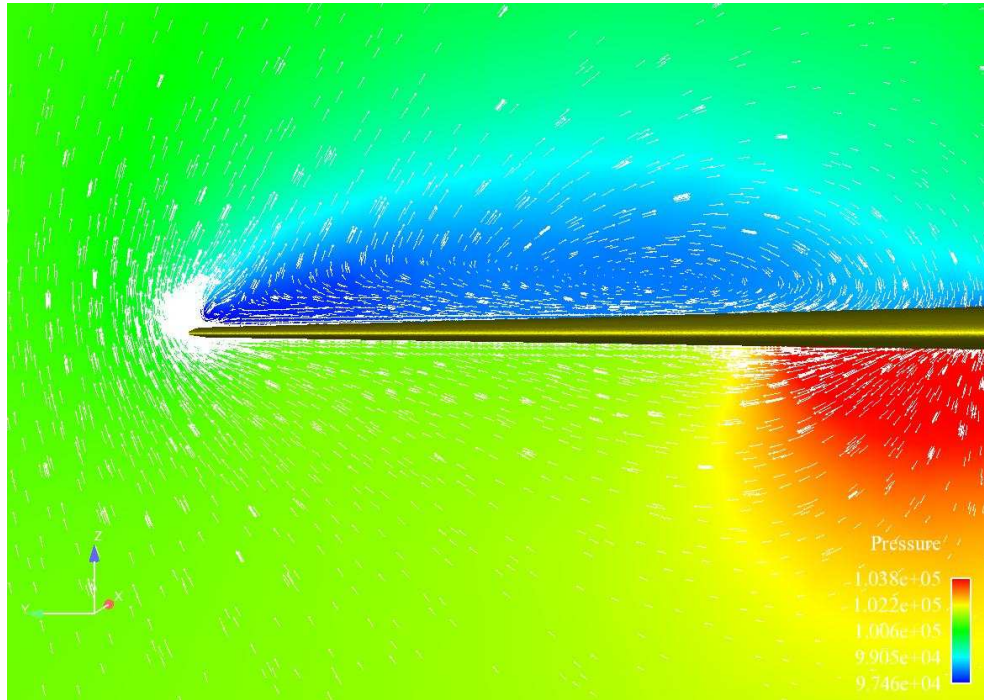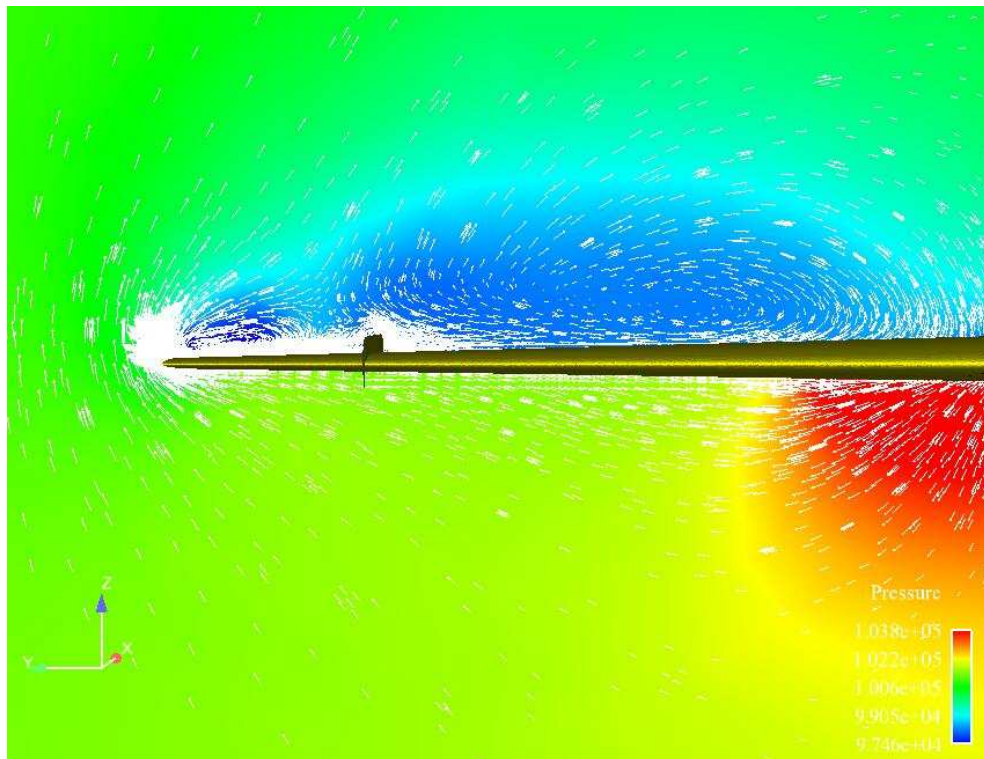
30
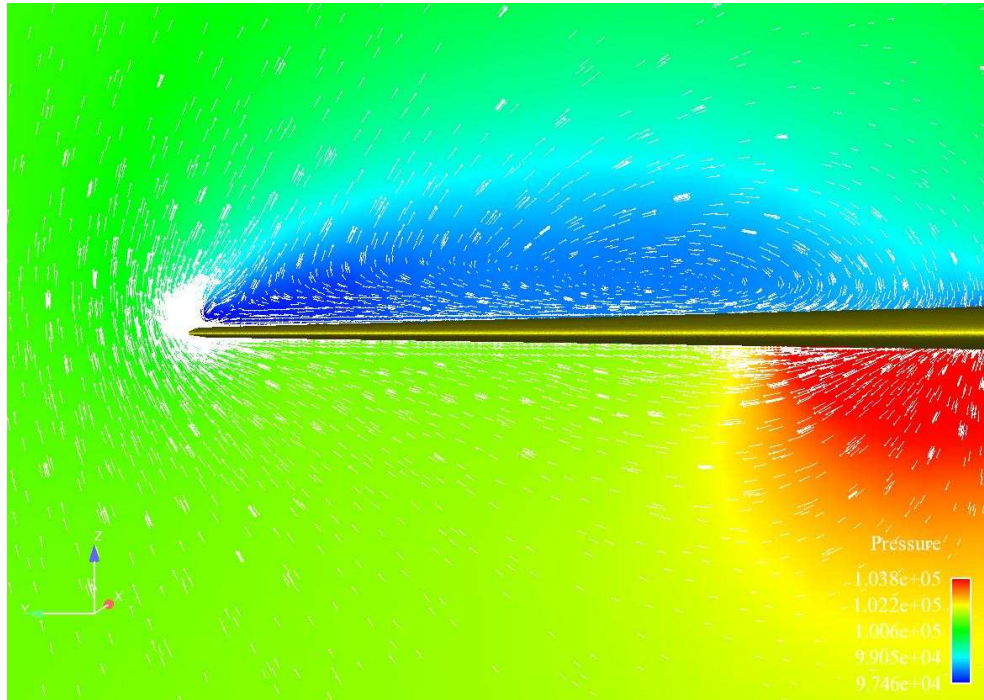
(a)
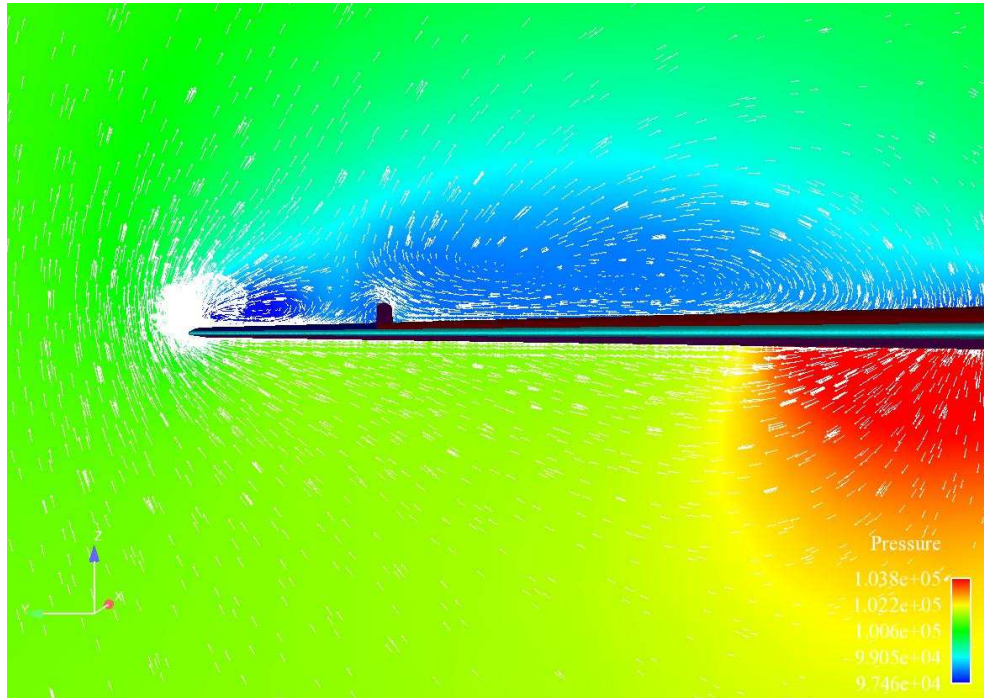
(b)

Figure 4.1:   (a) Flap only at 10° AOA.(b) Simple Fence at 10° AOA
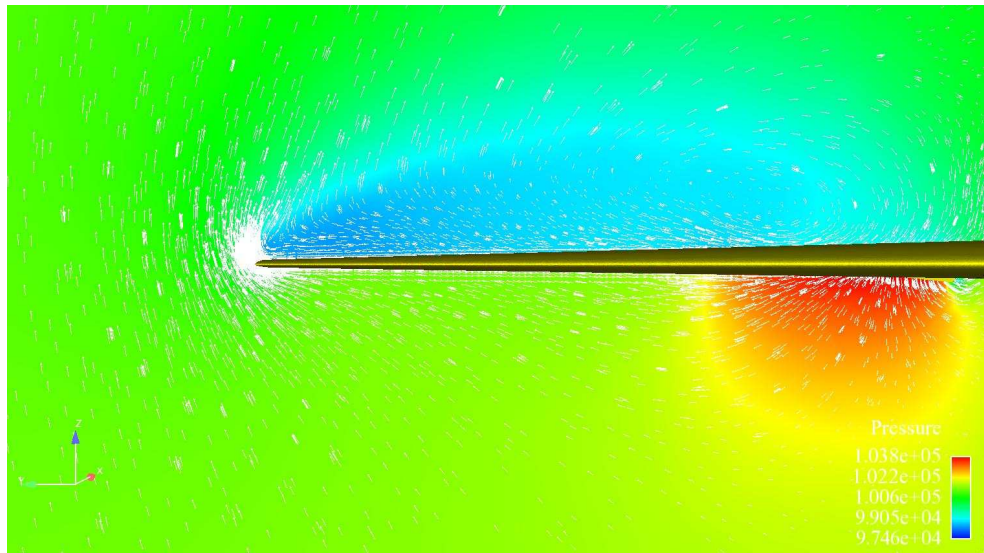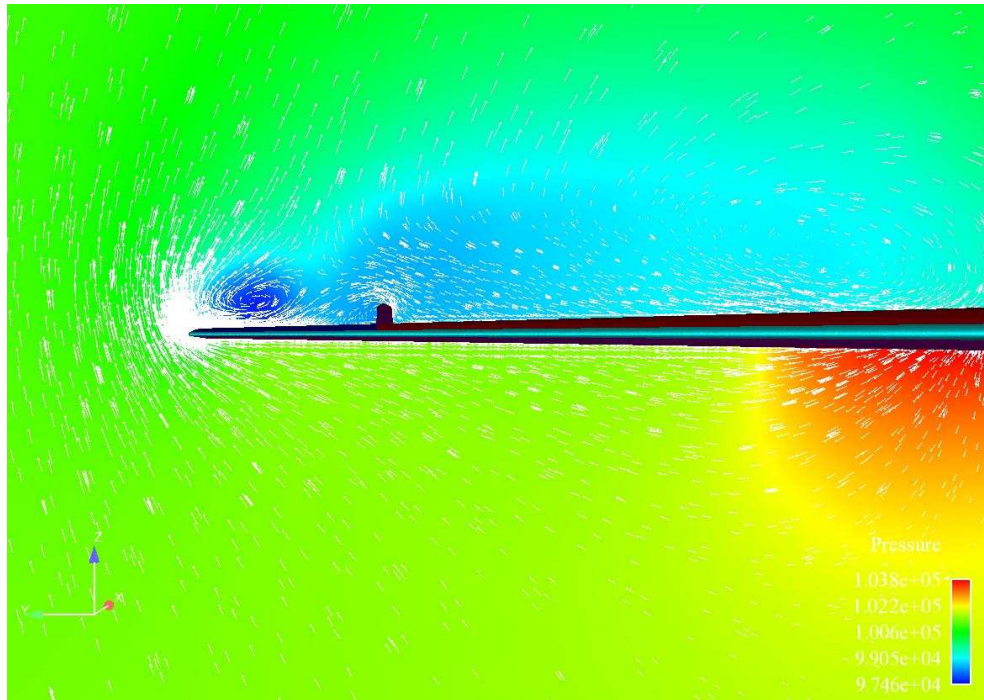
(a)

(b)

Figure 4.2:   (a) Flap only at 10° AOA.(b) Extended Fence at 10° AOA
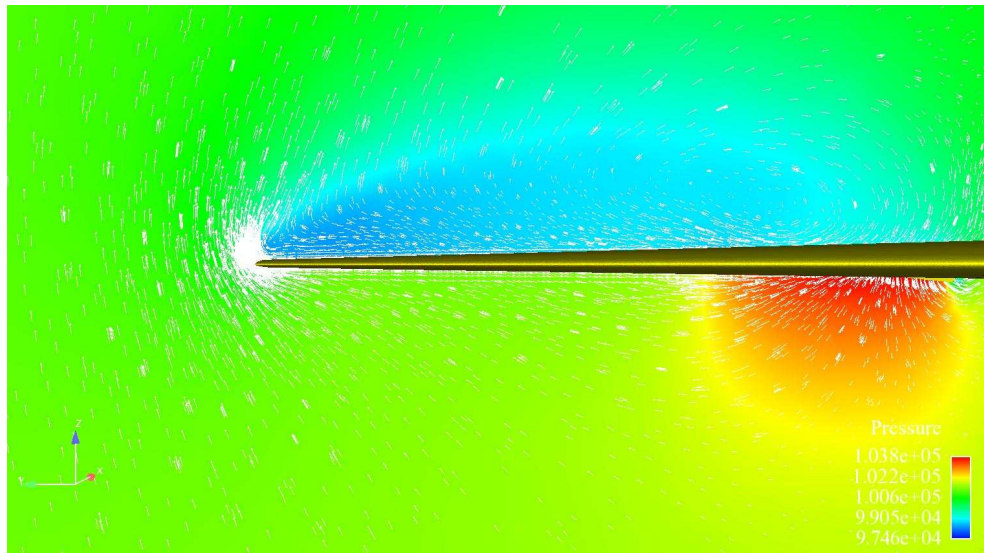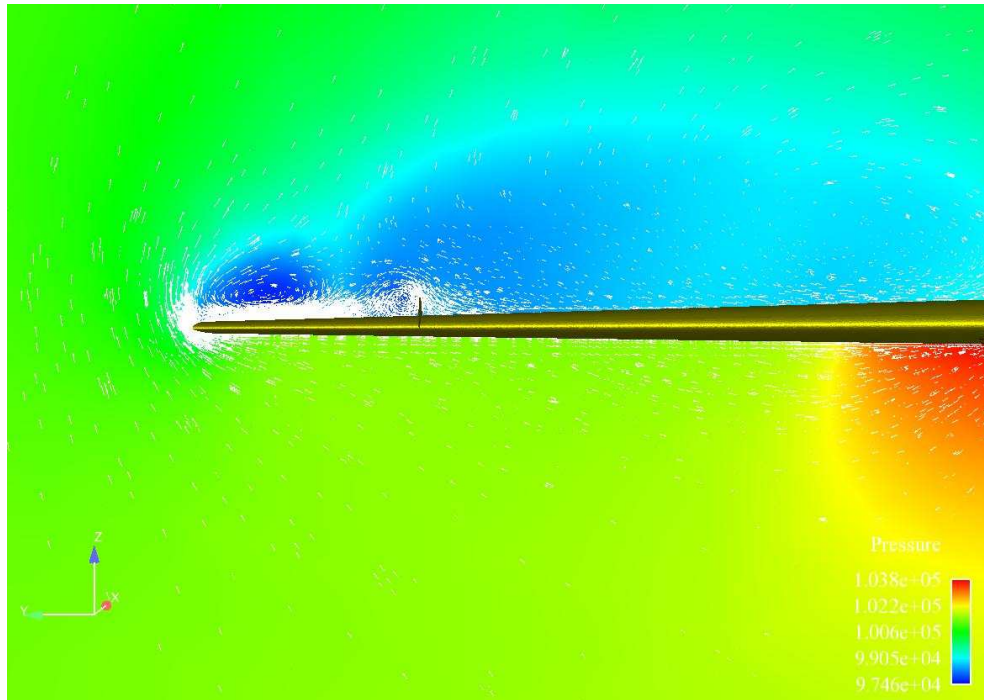
(a)

(b)

Figure 4.3:   (a) Flap only at 15° AOA.(b) Simple Fence at 15° AOA

(a)

(b)

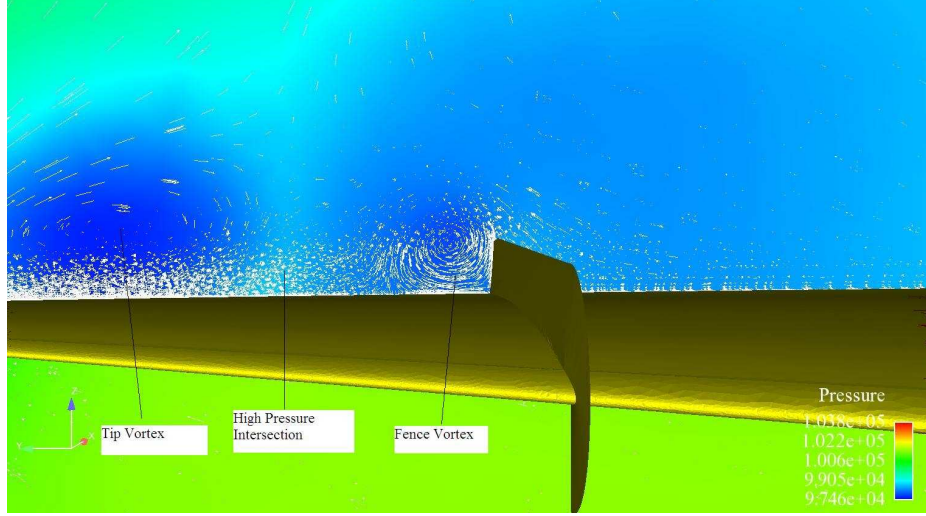Figure 4.4:   (a) Flap only at 15° AOA.(b) Extended Fence at 15° AOA

Figure 4.5:   Extended fence vortices at 15° AOA.

tip and fence vortices have opposite rotations. At the chord station used for the cut plane, the vortices appear to intersect and travel together towards the wing surface. This intersection appears to result in a thin region of higher pressure that divides the two low pressure regions.

4.3.1   Iso-Surfaces and Vorticity.   Although the X-cut planes revealed two vortices, they do not show how these vortices were generated, where they came from, or their strength. To gain further insight, iso-surfaces of total pressure were created. They give a three dimensional picture of the vortices and also a cursory idea of their respective strengths. Figure 4.6 shows the total pressure iso-surface at 98500 Pa for the extended fence and flap only solutions at 15° AOA.

Figure 4.6 confirms the low pressure regions observed in the X cut planes are generated by the fence. The tip vortex is created at the leading edge of the fence and shoots outboard towards the wing tip leaving a region of low pressure. The fence vortex follows the upper part of the fence, growing in size as it travels. At 98500 Pa, the iso-surface on the fence does not extend all the way to the leading edge. Rather it begins approximately 0.2 meter aft of the leading edge and increases in size as it moves along the chord towards the back of the wing. As it nears the end of the fence
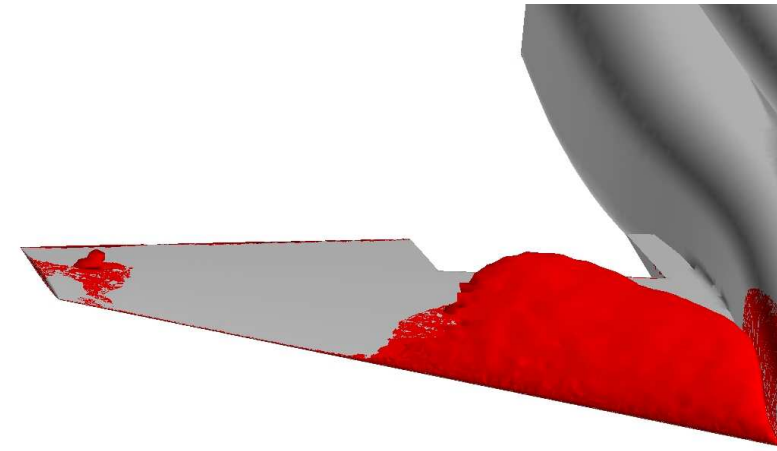
(a)

(b)

Figure 4.6:   (a) Flap only iso-surface at 98500 Pa and 15° AOA.(b) Extended Fence iso-surface at 98500 Pa and 15° AOA
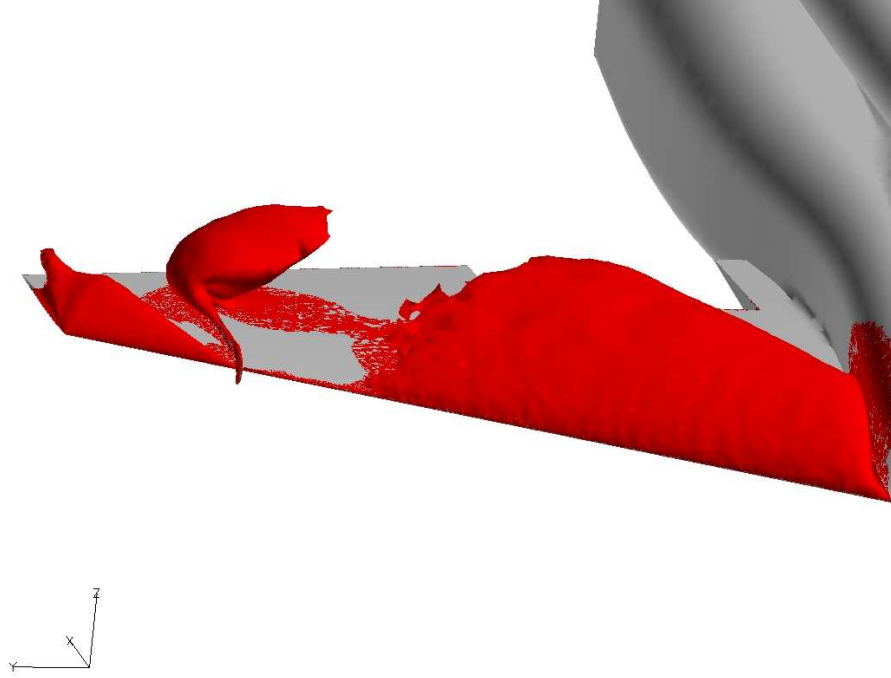
Figure 4.7:   Total pressure iso-surface at 98600 Pa and 15° AOA.

the vortex appears to burst. This is indicated by the sudden expansion of volume of the total pressure iso-surface. Figure 4.7 shows the same iso-surface view but at 98600 Pa. This visualization reveals the fence vortex begins at the leading edge and experiences the same bursting effect at approximately the same chordwise location on the fence.

4.3.2 Streamlines and Vorticity.   The iso-surface and X-cut visualizations are appropriate tools for looking at the three dimensional picture around the fence. They shed light into source of the vortices, and give a general impression of their strength and size. However, they fail to give quantitative results on the vortex strength and a full understanding on how the fence generates the vortices. To examine vortex strength and production, the vorticity magnitude was computed for the 15° AOA extended fence and flap only grids, and plotted with the streamlines in Figure 4.8.
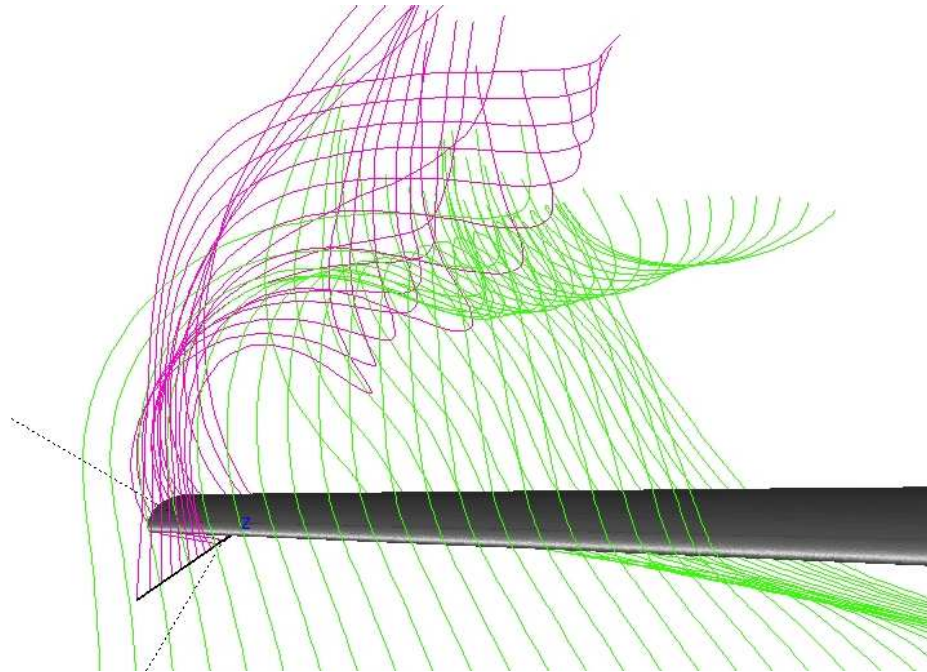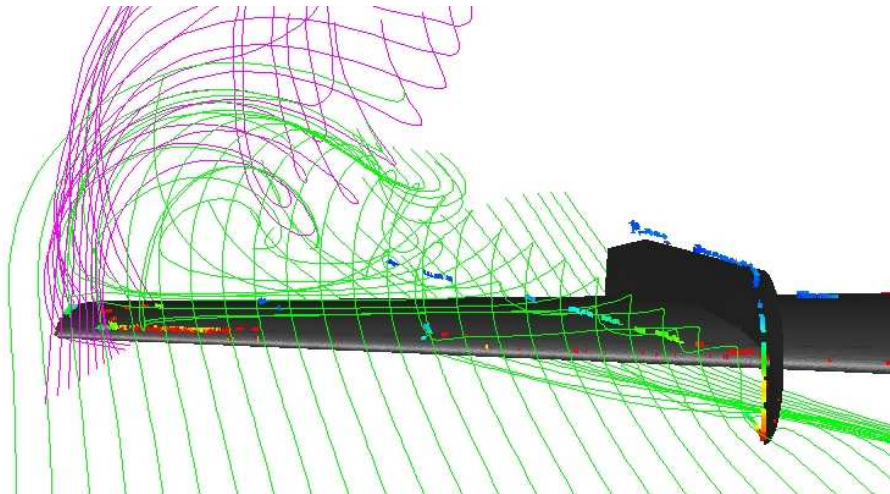
Figure 4.8:   (a) Streamlines and vorticity magnitude for a flap only at 15°(b) Stream-
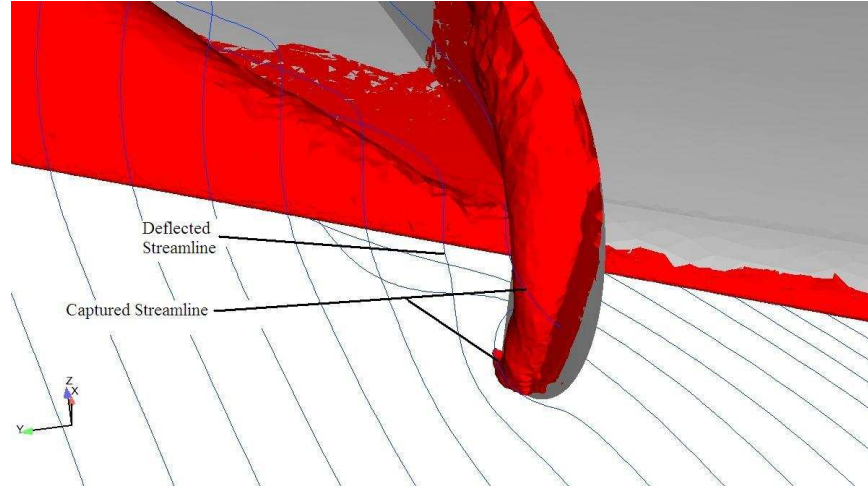lines and vorticity magnitude for an extended fence at 15°.

Figure 4.9:   Fence Vortex Source

The streamlines for the flap only configuration display normal behavior. Circulation around the wingtip is evident and there is a deflection of the streamlines towards the wingtip on the upper surface.

The fence visualization is significantly different. Two distinct vortex cores protrude from the leading edge and fence intersection. The first extends from the fence edge towards the wing tip and the other remains close to the fence. The location of the vortex cores is not surprising in light of the preceding iso-surface plots which predicted the vortices in the same locations. The color scale reveals the vortex traveling towards the wingtip is slightly stronger than the fence vortex over a greater portion of the wing.

The streamlines in Figure 4.8 reveal how the fence generates the vortices. Flow does not travel smoothly over the leading edge as it does in the flap only case. As air moves towards the fence it begins to deflect toward the wing tip in the same manner as the streamlines with no fence. However, the fence blocks this movement. The blocked flow causes a region of low pressure on the outboard side of the fence. This low pressure grabs the streamlines in its vicinity and does not allow them to continue towards the wing tip. Instead, these captured streamlines spin around the low pressure region and continue to the back of the fence trapped in the fence vortex.
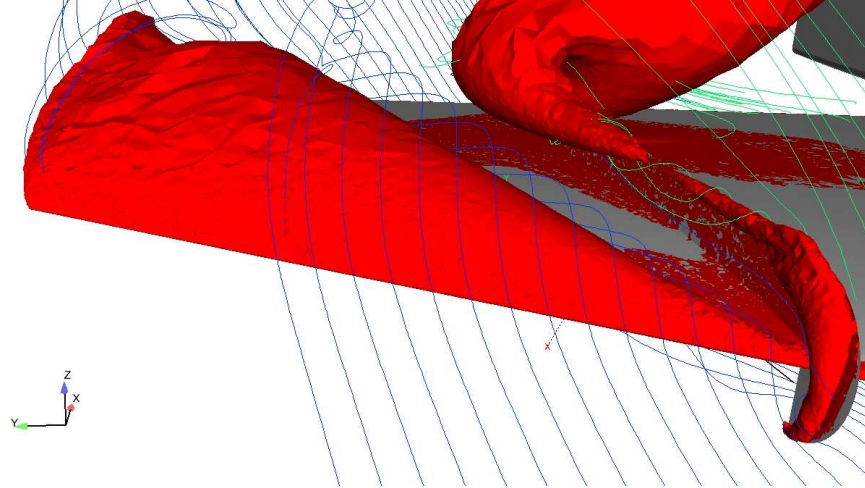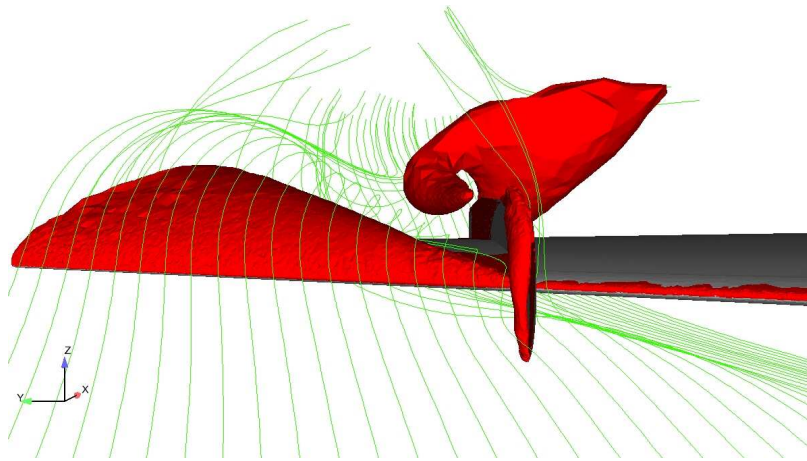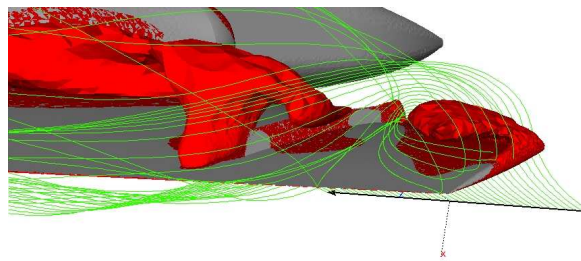
Figure 4.10:   Wing upper surface streamlines

Figure 4.9 shows an example of a streamline trapped by the fence vortex. Cross flow on the wing upper surface is also captured by the fence vortex. This effect is shown in Figure 4.10 where the green streamlines are coming from the inboard side of the fence and joining the fence vortex.

The tip vortex is also influenced by the fence, although in a more indirect fashion. The streamlines that are near the fence low pressure, but not captured by it, are still bent towards it. This can be seen in Figure 4.9. After this happens, the streamlines take a sharp turn towards the wing tip, and slide under the circulation from the high to low pressure on the wing tip. This interaction creates the tip vortex. Two views of this are observed in Figure 4.11. The reason the flow rapidly moves towards the wing tip is a result of blocked spanwise flow over the wing upper surface. Without the fence, cross flow exists because of a pressure gradient forcing air towards the wing tip. [23] With the fence, that same pressure gradient still exists. However, now cross flow on the upper wing surface that used to travel to the low pressure near the wing tip is blocked by the fence and wrapped into the fence vortex. Flow outboard of the fence must fill the void and rapidly travels towards wing tip. That movement results in the tip vortex in Figure 4.11. Figure 4.12 displays an oil flow around the fence showing the blocked spanwise flow.

(a)

(b)

Figure 4.11:   (a) Front view of the streamlines sharply curving towards the wing tip.(b) View of streamlines circling around low pressure iso-surface.
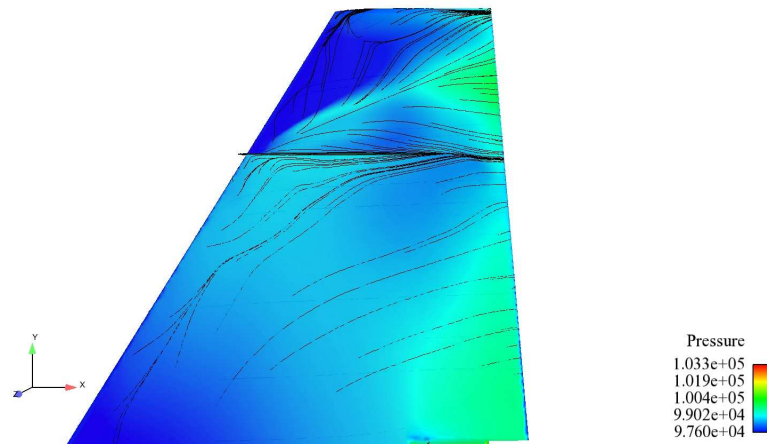

Figure 4.12:   Outboard wing upper surface streamlines

4.4   Pressure and Lift Distribution

The flow structure generated by the fence is important to understand. However, it is also important to determine its influence on lift. Figure 4.13 compares the pressure distribution on the wing with and without a fence at 15° AOA.

The fence produces a distinct alteration of the pressure distribution. Inboard the fence, the contours are roughly the same. Flow in both cases is beginning to separate near the wing root and trailing edge of the wing. Outboard of the fence, however, the pressure contours are markedly different. Although the flow on the outboard portion of the wing is attached without a fence, pressure is significantly lower when the fence is present. This indicates the flow is more resistant to separation than it would be without the fence. This appears to be a direct result of the vortices generated by the fence energizing the flow. There are two regions of low pressure created by the vortices. The most intense low pressure region protrudes from the front of the fence towards the wing tip. A second, less intense, low pressure section remains close to the outboard side of the fence. Figure 4.14 shows how the low pressure on the wing corresponds to the fence and tip vortices.

A visual inspection of Figures 4.13 and 4.14 indicate the fence creates significant areas of low pressure which increases the lift at a given AOA. However, a visual inspection of this kind is not fully adequate. To quantify the fence's influence on lift, cut planes running chordwise were intersected with the wing at six locations. These intersections created a line where pressure data could be extracted and integrated. The six locations are shown in Figure 4.15.

The pressure data was imported into Matlab™, converted to C_p, and integrated over the length of the chord giving the C_n. The C_n is roughly proportional to the sectional lift coefficient. [3] The result at each section was normalized by the root chord and shown in Figure 4.16. The C_n average value with no fence is 0.41. It has a value of 0.435 at station 6 and decreases linearly towards the wing tip. The average C_n with the fence is 0.465 and does not decrease in the same pattern. Figure 4.16
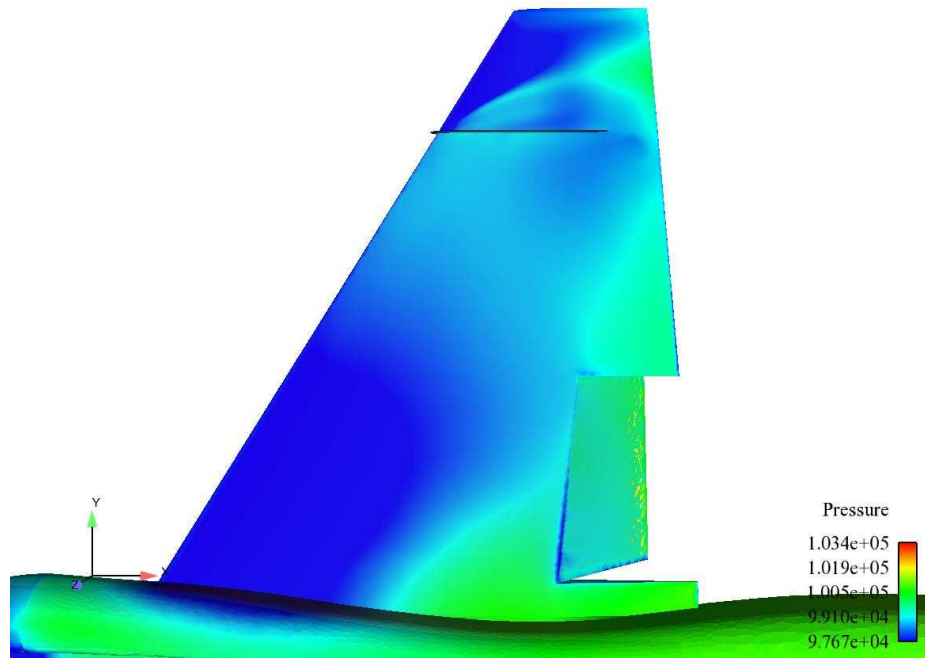
(a)
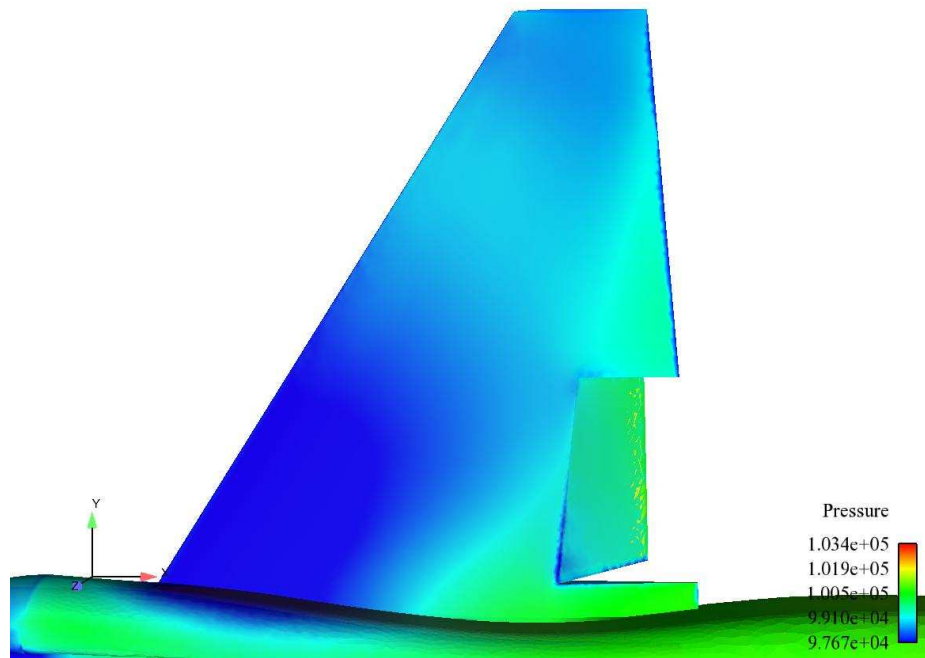
(b)

Figure 4.13:   (a) Pressure on the wing with an extended fence at 15°.(b) Pressure on the wing with a flap only at 15°
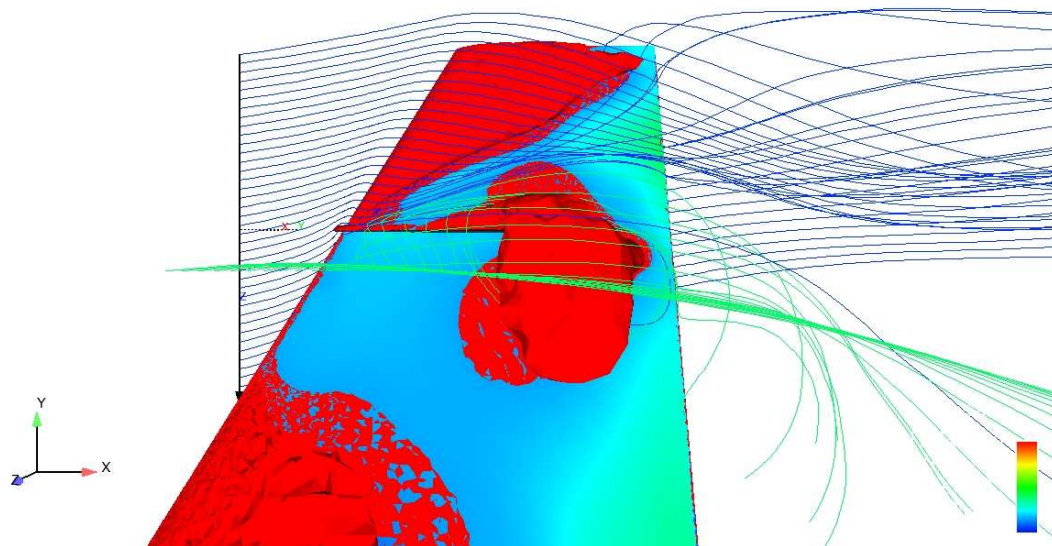
43

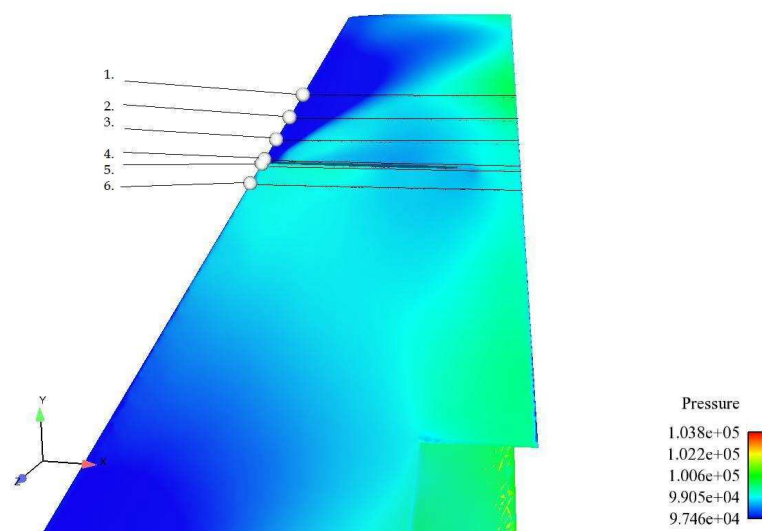Figure 4.14:   Wing surface with iso-surfaces, pressure contours, and streamlines.

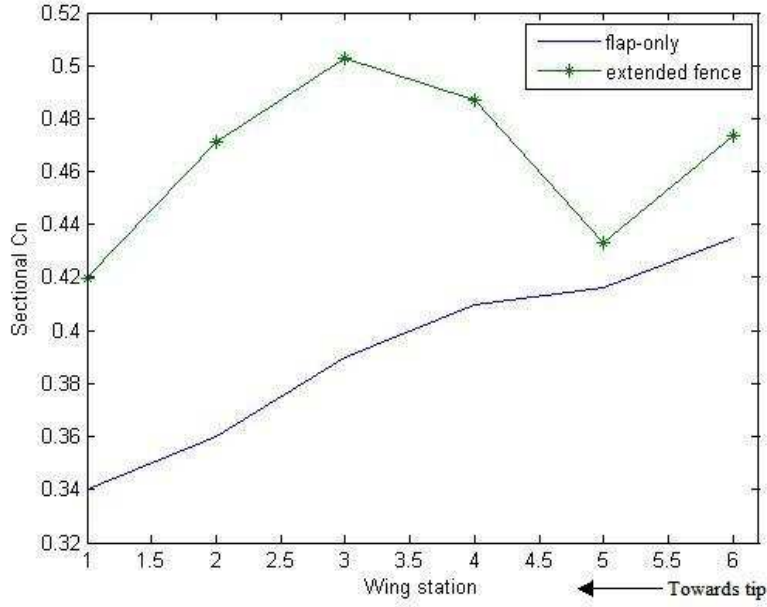Figure 4.15:   Pressure data extraction points.

Figure 4.16: Sectional C_n at each wing station for the extended fence and flaps-only configurations.

demonstrates the C_n is higher at each wing station than it is with no fence. At station 4 the C_n was increased by 16% and at station 3 it was increased by 22%. These are significantly higher and prove the fence is increasing lift on the outer portion of the wing.

4.4.1 Effect of AOA on Fence Performance. The extended fence produced a 4.9% increase in the C_L at 15° angle of attack. However, the same grid and fence produced only a 1.1% increase at 10° AOA. There is a trend towards a decrease in effectiveness at lower AOA in every grid and fence type. Table 4.3 compares the percentage increase in C_n for the 10° and 15° extended fence from the flaps only case. The results reveal the increase in C_n is lower at 10° than at 15° AOA. As an example, at 10°, C_n increases at stations 3 and 4 by 13% and 1.8%, respectively. At 15°, the increase at the same locations is 22% and 13%. At stations 5 and 6 the C_n actually decreases by 5% and 1.7% at 10° AOA. These results indicate the fence vortices are not as effective in energizing the flow at lower AOA.

Table 4.3:   Increase in C_n in the presence
of a fence at 10° and 15°

| Wing Station	% Increase at 10°	%Increase at 15°
1	11	19
2	14	23.5
3	13	22
4	1.8	13
5	-5	4
6	-1.7	8

4.4.2 Influence of Fence Type.   The extended fence produced the greatest change in C_L. As an example, the simple fence increased C_L by 0.9% at 15° AOA while the C_L with an extended fence increased 4.9%.

Figure 4.17 examines the vortex core strength by plotting the vorticity magnitude for each fence type at 15° AOA. The same color scale for both cases is used. The vortex cores created by the extended fence are well defined. The tip vortex begins at the leading edge and travels towards the wing tip. The fence vortex core follows the leading edge of the fence around towards the back of the wing. With a simple fence neither vortex is easily distinguished or as strong as the extended fence vortices. Instead of beginning at the leading edge, the fence vortex starts 4" aft of fence edge and is weaker and more chaotic. The tip vortex is almost non existent. Figure 4.18 shows the path that the streamlines take around the simple fence. The streamlines close to the fence are not caught by the low pressure area on the outboard side of the fence. Figure 4.9, in Section 4.3.2, shows the streamlines in the same vicinity being trapped into the fence vortex. The simple fence loses effectiveness because its vortices are weaker than those from the extended fence.
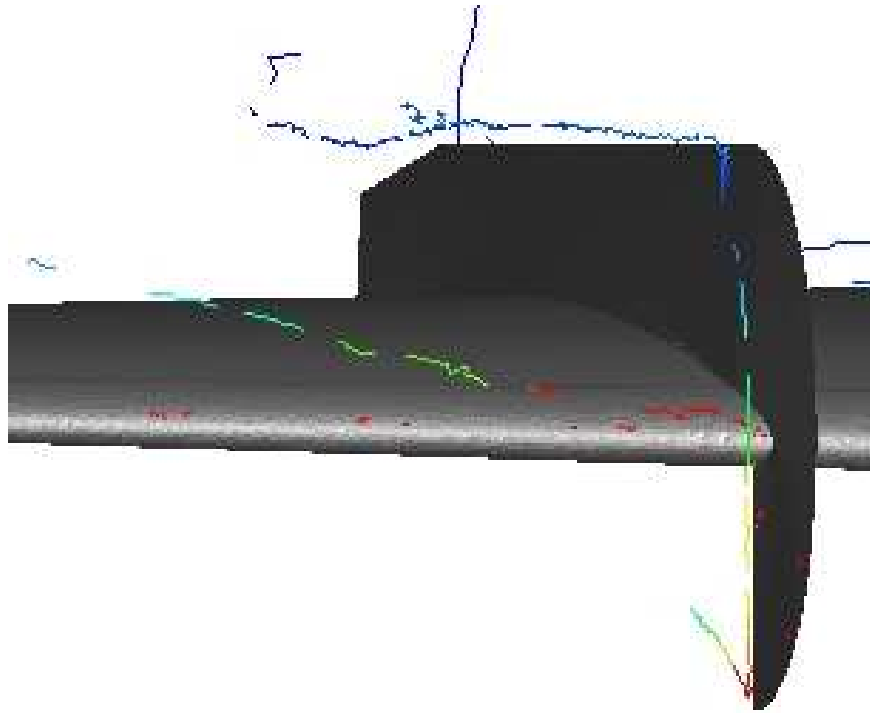
(a)
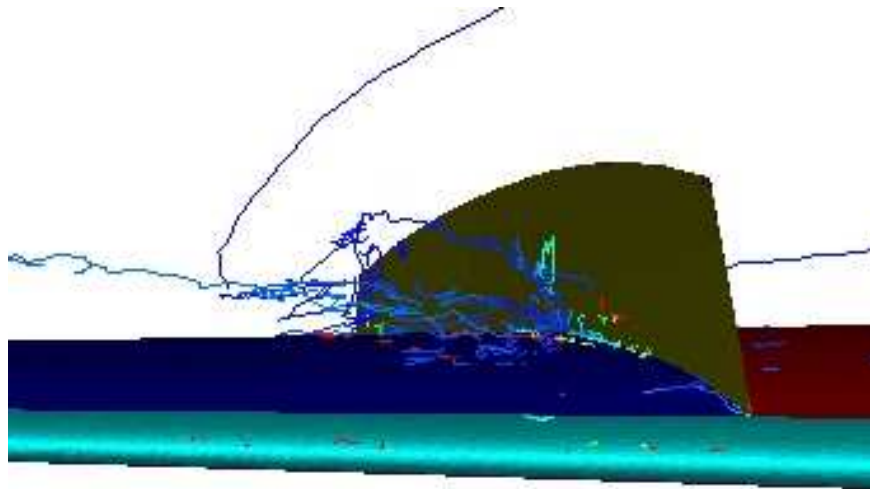
(b)

Figure 4.17:   (a) Extended fence vortex core magnitude at 15°.(b) Simple fence
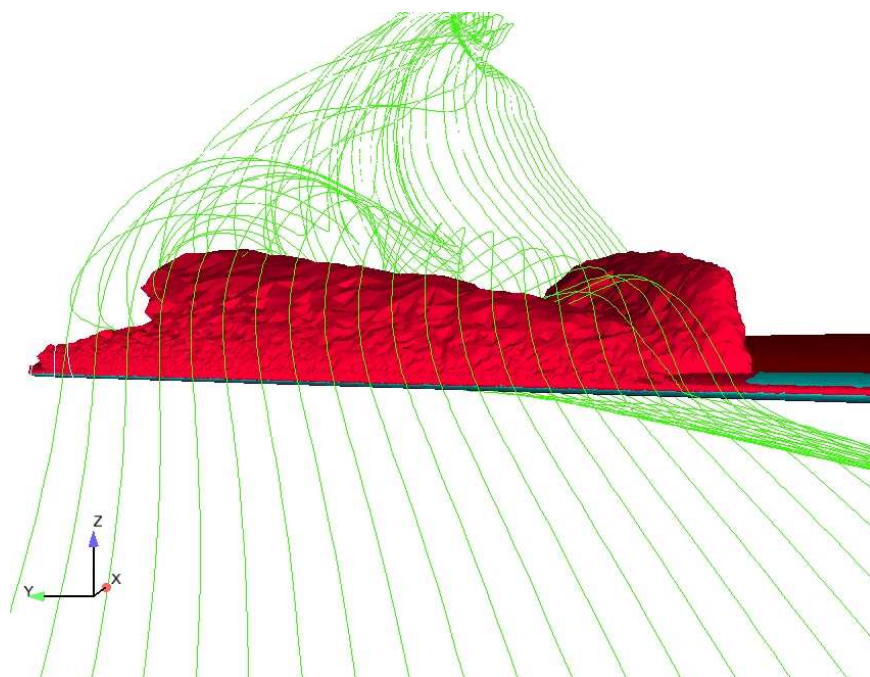vortex core magnitude at 15°

Figure 4.18:   Simple Fence Streamlines.

V. Conclusions

5.1 Contributions to the Current Fence Theory

The understanding of the wing fence was improved by this study. Chapter 2 outlined the current wing fence theories. Those theories do an adequate job of explaining the fence by discussing its effects on the potential flow and the presence of vortices. However, it did not adequately explain how the vortices are produced, why wrapping the fence around the leading edge is more effective, the effect of fence size, or a clear link between the vortices and the potential flow.

5.1.1 Wing Fence and Vortices.

Zhidkosti's study revealed the wing fence produced two vortices. One was generated along the upper portion of the fence on the inboard side. This vortex was produced by a pressure differential across the fence. Zhidkosti's work did not determine the location or the source of the other vortex. [23] The current study not only detected both vortices, but revealed the location and source of the second vortex, and the vortice's effects on lift. The fence vortex location and source was very similar to Zhidkosti's work. It formed on the upper portion of the fence due to a pressure differential, and traveled towards the back of the wing remaining close to the fence. The only difference was it formed on the outboard side of the fence. This could be an effect of the wing sweep angle. The T-38 quarter chord is swept 24° and the whole wing in Zhidkosti's work was swept 55°.

The second vortex was generated as a result of the fence vortex. CFD visualizations revealed the fence does not merely slow the spanwise flow, but captures it in the fence vortex. The flow captured by the fence vortex does not continue to travel towards the low pressure region near the wing tip. The flow outboard of the fence rushes towards the low pressure region on the wing tip to fill the void, forming the second vortex. Figure 5.1 gives an excellent view of both vortices and their effects. Streamlines intersecting the leading edge of the wing near the fence are caught in the fence vortex, which is fed by the spanwise cross flow coming over the top of the fence.
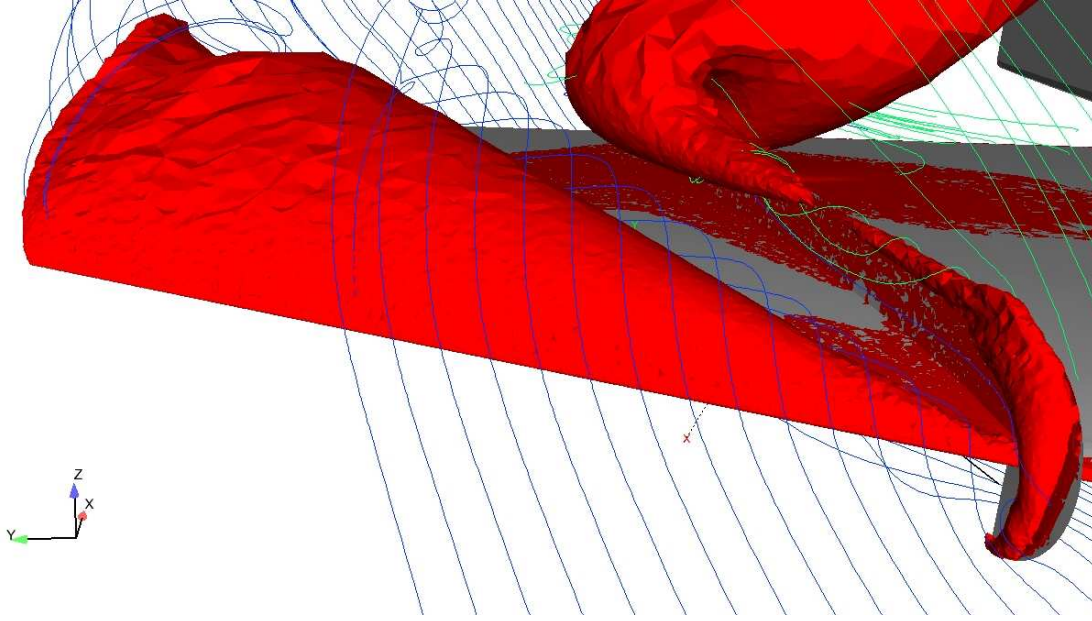
49

Figure 5.1:   Simultaneous fence vortex production.

The streamlines that are not trapped by the fence vortex, quickly shoot towards the wing tip to fill the void created by the lack of cross flow in the boundary layer.

The vortices generated by the fence energize the flow. This lowers the pressure on the upper wing surface outboard of the the fence as shown in Figure 4.13

Although the fence is increasing the effective C_L, the way the fence is working is different than the theory predicted. The research in Chapter 2 stated a fence works because it decreases the lift load outboard of the fence, thus delaying wing tip stall. [16] However, the C_n distribution in Figure 4.16 indicates the lift load on the T-38 wing is increased outboard of the fence. The departure from theory is a result of the T-38 fence vortices energizing the flow around the fence and decreasing pressure on the upper surface of the wing.

5.1.2   Effect of Wing Fence Shape and Size.   The effectiveness of the extended fence was substantially increased by wrapping the fence around the leading edge which increased the strength of the fence vortex. The stronger fence vortex resulted in a stronger tip vortex. These vortices lowered the pressure on the upper surface of the

50

wing more than a simple fence. The Figures included in section 4.17 provide a visual example of the different effects of the two fence geometries.

Although the height of the fence was not directly tested, the results shed light into the importance of the fence height. Previous studies have demonstrated if a fence is too small, it will not be effective. [16] The streamlines in Figure 5.1 show that cross flow comes over the fence towards the wing tip and gets trapped by the fence vortex. If the fence was short, it is likely the fence vortex would either be too weak to capture the cross flow or not exist at all. It can be speculated without the fence vortex, the tip vortex may not exist, and the flow would appear essentially the same as if it had no fence.

5.2   *Future Research and Recommendations*

As with most experiments, the results of this research lead to more questions and ways the wing fence could be studied more effectively. RANS served its purpose in this study by capturing the mean effects of the fence. However, it may have fallen short in accurately determining unsteady effects near stall. As previously stated, current CFD research has lead to the conclusion that DES captures stall and unsteady effects better than RANS. [11] Any future CFD fence research into the wing fence should use DES or a similar time accurate method. Also, this research did not address two important topics; drag and Mach effects. The T-38 is a supersonic aircraft and the effects of the fence in this regime could be significant. The fence could also increase drag to the point where its lift benefits are not worth the drag penalty. Drag induced by the fence should be an important consideration in the future.

There is concern the fence could negatively effect the structural integrity of the wing. When the T-38 was designed, it did not include the wing section outboard the fence. It was added to increase the lifting surface. The fence will generate loads which could change the natural frequency of the wing. [23] Any one of these effects could produce unforseen negative consequences. Future research should study the structural influence of the fence.

It is very difficult to spin the T-38 since it was designed to stall before spinning. This is an important feature because once the T-38 enters a spin, it is unrecoverable. The fence's effectiveness could theoretically prove fatal by allowing the T-38 to shoot past its $C_{L_{max}}$ and enter an uncontrollable spin. This issue should be carefully examined before flight test.

5.3 Final Thoughts

This study was successful on two levels. First, it took a large step into understanding the complicated relationship between the cross flow, vortices, lift distribution, and the overall effects of a wing fence. It revealed the source of both fence vortices, and gave a better understanding of the effects of fence shape and size. Second, it demonstrated the strong likelihood an extended wing fence will be beneficial to the high AOA flight characteristics of the T-38. It will be exciting to see the results of the flight test phase of the wing fence study.

Appendix A. Supplemental Discussions and Data

This Appendix includes a discussion of the application of DES solutions to the wing fence and the MATLAB® script used for calculating the C_n.

A.1 Discussion of DES

The flow in the regime where the wing fence is effective is turbulent and unsteady. Research has shown that there are limitations with RANS turbulence models when they are applied to highly unsteady, separated flows. [15] RANS can produce too much eddy viscosity which damps out the unsteady nature of the flow. [17] To combat this, techniques have been developed to accurately account for the correct eddy viscosity. One successful method for solving unsteady flows is to filter the RANS equations so that the eddy viscosity does not include the energy of the grid resolved turbulent scales. [15] This model is called Large Eddy Simulation, LES. LES operates on two assumptions. The first is that the transport of flow properties is mostly contained in large eddies and that the small scale flow features can be modeled by a Sub Grid Scale, SGS, model. [13] In other words LES uses the Navier Stokes equations to directly model the largest eddies, and a SGS to account for the energy contained in the smallest eddies. LES has shown large improvements over basic RANS formulations when compared to experimental data, however, it's gridding requirements are on the scale of the Reynolds number squared.

The major limitation of LES is that in the boundary an extremely high grid density must be used to capture the flow properties. DES is designed to gain the benefits of LES to model time dependent, three-dimensional turbulent flow, while using RANS within the boundary layer to lower grid requirements. DES switches between LES and RANS based on the grid density. AVUS is capable of computing DES solutions. It uses the S-A RANS model in the boundary layer and switches between RANS and LES based on the grid density. [2] Future CFD research into the T-38 should use DES. It is difficult to determine with certainty how a DES would in-

fluence the results, however, given the current success of DES, it would be a beneficial experiment.

A.2 Matlab Script

```
clear; clc;;
for i = 6
  name = ['cp' i_name];
  fid = fopen(name);
   data{i} = fscanf(fid,'%g %g',[2 inf]);
   x = data{i}(1,:);
   P = data{i}(2,:);
end
 max(x)/2
lengthx=length(x)
%VALUES FOR LOW DEN EXT FENCE N=90, -300
n=90 q=length(x)-300

xfind=x(n:q);
%define temp pressure to get the min indices
%[xfindnew,I]=min(xfind)

presfind=P(n:q); [xfindnew,I]=min(presfind);

endxlow=I+n; startxhigh=endxlow

%Define Xlower and Xupper
%IF GETTING DISTINCT ERROR!!!!!!!!!!!!!!!! rand
```

```
n=0 xlower=x(1:endxlow); xupper=x(startxhigh:lengthx);
%Correct for repeated entries
for u=1:length(xupper) xupper(u)=xupper(u)+.001*rand; end for
u=1:length(xlower) xlower(u)=xlower(u)+.001*rand; end
%Define Pu Pl
Pl=P(1:endxlow-n); Pu=P(startxhigh-n:lengthx);
plot(xlower,Pl,'r',xupper,Pu)


%Convert to Cp
Po=101325; M=0.2; a=340; V=M*a; row=1.225; Cpl=(Pl-Po)/(.5*row*V^2);
Cpu=(Pu-Po)/(.5*row*V^2);


%plot(xlower,Cpl,xupper,Cpu)


%now interpolate
xnewlower=0:0.01:(max(x)/2); lxnewlow=length(xnewlower);
xnewupper=(max(x))/2 :   (-max(x)/2+(max(x)))/lxnewlow :  (max(x));
xnewupper=xnewupper(1,2:length(xnewupper));


Cplint=interp1(xlower,Cpl,xnewlower);
Cpuint=interp1(xupper,Cpu,xnewupper);


%redefine first element of Cpuint
%Cpuint(1)=Cplint(length(xnewlower));
%Correct the Lengths
%Cpuint=Cpuint(1:(length(Cpuint)-1));
%then subract values to get a delta Cp


%plot(xnewlower,Cplint,xnewupper,Cpuint)400
```

```
plot(xnewlower,Cplint,'r',xnewlower,fliplr(Cpuint),'g')
%Cplint=fliplr(Cplint)
Cpuint=fliplr(Cpuint);
Cp=Cplint-Cpuint;
%plot(xnewlower,Cp)


Cl=0
r=2
    for m=1:length(xnewlower)-r;
        Clp(m)=Cp(m)*(xnewlower(m+1)-xnewlower(m));
    end

Cl=sum(Clp(1,2:length(xnewlower)-r))/2.7
```

Bibliography

1. Air Force Research Laboratory, Wright Patterson AFB, OH. *Solid Mesh Manual*, 2005.

2. Air Force Research Laboratory, Wright Patterson AFB, OH. *Air Vehicles Unstructured Solver*, January 2006.

3. Anderson, John D. *Introduction to Flight*. McGraw-Hill Higher Education, Madison, Wi, fourth edition edition, 2000.

4. Anderson, John D. *Fundamentals of Aerodynamics*. McGraw Hill Higher Education, New York, NY, third edition edition, 2001.

5. Banks, Carl. "Boundary Layer", www.aerojockey.com 1999.

6. Barrett, Ron and Saeed Faokhi. "On the Aerodynamics and Performance of Active Vortex Generators". *AIAA-93-23447-CP*, 376–386, 1993.

7. Caspers, Captain Matt. *CFD Investigation of Flow Past Idealized Engine Nacelle Clutter*. Master's thesis, Graduate School of Engineering, Air Force Institute of Technology, Wright-Patterson AFB OH, March 2007. AFIT/GAE/ENY/07J-M08.

8. Chambers, Joseph R. "Concept to Reality". *NASA*, February 2007.

9. Cummings, Russell, James R. Forsythe, Scott A. Morton, and Kyle D. Squires. "Computational Challenges in High Angle of Attack Flow Prediction". *Progress In Aerospace Sciences*, 369–384, September 2003.

10. Forsythe, James R., Kyle D. Squires, and Aroon K. Viswanathan. "Detached-Eddy Simulation around a Forebody at High Angle of Attack". *AIAA Aerospace Sciences Meeting*, January 2003.

11. Forsythe, James R., Kyle D. Squires, Kenneth Wurtzler, and Philippe R. Spalart. *Journal Of Aircraft vol. 41 No. 2*.

12. Forsythe, James R., Kyle D. Squires, Kenneth Wurtzler, and Philippe R. Spalart. "Detached-Eddy Simulation of the Fighter Aircraft at High Alpha". *AIAA 2002-0591*, January 2002.

13. Grinstein, Fernadno F. and Christer Fureby. "Implicit Large Eddy Simulation of High-Re Flows with Flux-Limiting Schemes". *AIAA Computational Fluid Dynamics Conference*, June 2003.

14. Lin, J.C., G.V. Selby, and F.G. Howard. "Exploratory Study of Vortex-Generating Devices for Turbulent Flow Separation Control". *AIAA 91-0042*, January 1991.

15. Nichols, Robert H. "Turbulence Models and Their Application to Complex Flows". *Mississipi State University*, 2001.

16. Nickel, Karl and Micahel Wohlfahrt. *Tailless Aircraft*. American Institude of Aeronautics and Astronautics,Inc., New York, NY, first edition edition, 1994.

17. Spalart, Philippe R. "Young-Persons's Guide to Detached-Eddy Simulation Grids". *Nasa/CR-2001-211032*, July 2001.

18. United States Air Force. *T-38A Flight Manual*, August 2005.

19. United States Air Force, http://www.airforce-technology.com/projects/t-38/. *T-38*, 2007.

20. United States Army. *Fundamentals of Gas Turbine Engines*.

21. Vavilis, Panagiotis S. and John A. Ekaterinaris. "Computational Investigation of Flow Control over Wings". *AIAA Aerospace Sciences Meeting and Exhibit*, 369–384, January 2007.

22. Wikipedia, www.wikipedia.com/wingfence. *Photo of Mig with a wing Fence*, 2007.

23. Zhidkosti, Mekhanika. "Flow on a Swept Wing in the Region of a Fence". *Journal of Fluid Dynamics Vol. 3 No.6*, 84–86, July 1968.

1. REPORT DATE *(DD-MM-YYYY)* 14-06-2007	**2. REPORT TYPE** **Master's Thesis**	**3. DATES COVERED** *(From – To)* **June 2006– June 2007**
4. TITLE AND SUBTITLE CFD Analysis of a T-38 Wing Fence		**5a. CONTRACT NUMBER**
		5b. GRANT NUMBER
		5c. PROGRAM ELEMENT NUMBER
6. AUTHOR(S) Solfelt, Daniel, A., Ensign, USN		**5d. PROJECT NUMBER**
		5e. TASK NUMBER
		5f. WORK UNIT NUMBER

7. PERFORMING ORGANIZATION NAMES(S) AND ADDRESS(S)
  Air Force Institute of Technology
  Graduate School of Engineering and Management (AFIT/EN)
  2950 Hobson Way
  WPAFB OH 45433-7765
		8. PERFORMING ORGANIZATION REPORT NUMBER
		
		AFIT/GAE/ENY/07-J19

9. SPONSORING/MONITORING AGENCY NAME(S) AND ADDRESS(ES) n/a		**10. SPONSOR/MONITOR'S ACRONYM(S)**
		11. SPONSOR/MONITOR'S REPORT NUMBER(S)

12. DISTRIBUTION/AVAILABILITY STATEMENT   APPROVED FOR PUBLIC RELEASE; DISTRIBUTION UNLIMITED.

13. SUPPLEMENTARY NOTES

14. ABSTRACT
A computational study of the effects of a wing fence on the T-38 Talon was performed. RANS simulations were conducted using the CFD solver AVUS to examine the flow around the T-38 and the fence at a Reynolds number of 10 million. The T-38 was modeled as a half aircraft with a symmetry plane down the center line and did not include the empennage. The engine inlet and exhaust were modeled as sink and source boundary conditions using mass flow and pressure specifications. Two fence geometries placed 26" from the wing tip were tested. The first fence, called a simple fence, ran chordwise on the upper surface of the wing. It did not produce significant benefits. The second fence geometry, called the extended fence, wrapped around the leading edge of the wing and produced a 4.9 % increase in the lift coefficient at 15 degrees angle of attack. It was found that the vortices generated by the fence energized the flow outboard the fence, increasing lift. The extended fence generated vortices significantly stronger than the simple fence, resulting in a higher lift coefficient at 15 degrees angle of attack. These findings indicate that the T-38 high angle of attack performance would be improved by the addition of an extended wing fence.

15. SUBJECT TERMS
Wing fence, T-38 Talon, Reynolds averaged Navier Stokes, computational fluid dynamics, AVUS, vortices,

16. SECURITY CLASSIFICATION OF:			**17. LIMITATION OF ABSTRACT**	**18. NUMBER OF PAGES**	**19a. NAME OF RESPONSIBLE PERSON** LtCol Raymond C. Maple
REPORT **U**	**ABSTRACT** **U**	**c. THIS PAGE** **U**	UU	72	**19b. TELEPHONE NUMBER** *(Include area code)* (937) 255-3636, ext 4577